SYNTHESIS AND CHARACTERIZATION OF POROUS SODIUMALUMINOSILICATE DECORATED WITH NICKEL AND PALLADIUM

BY

Naila Haroon

Reg. No. 00000203210

DEPARTMENT OF CHEMISTRY

SCHOOL OF NATURAL SCIENCES (SNS)

NATIONAL UNIVERSITY OF SCIENCES AND TECHNOLOGY (NUST)

ISLAMABAD, PAKISTAN

2019

SYNTHESIS AND CHARACTERIZATION OF POROUS SODIUMALUMINOSILICATE DECORATED WITH NICKEL AND PALLADIUM

BY

Naila Haroon

Reg. No. 00000203210

A thesis submitted in partial fulfillment of the requirements for the degree

of

Master of Science

in

Chemistry

DEPARTMENT OF CHEMISTRY
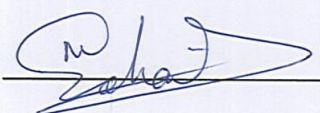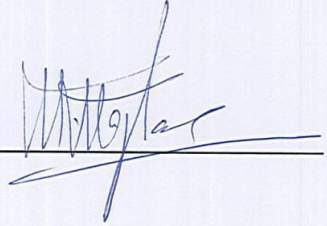
SCHOOL OF NATURAL SCIENCES (SNS)

NATIONAL UNIVERSITY OF SCIENCES AND TECHNOLOGY (NUST)

ISLAMABAD, PAKISTAN

2019

National University of Sciences & Technology

MS THESIS WORK

We hereby recommend that the dissertation prepared under our supervision by: <u>Naila Haroon,</u> Regn No. <u>00000203210</u> Titled: <u>Synthesis and Characterization of Porous Sodium aluminosilicate Decorated with Nickel and Palladium</u> be accepted in partial fulfillment of the requirements for the award of **MS** degree.

Examination Committee Members

1. Name: <u>DR. AZHAR MAHMOOD</u>   Signature: _____

2. Name: <u>DR. MANZAR SOHAIL</u>   Signature: _____

External Examiner: <u>DR. MUHAMMAD SHER</u>   Signature: _____

Supervisor's Name <u>PROF. M. MAZHAR</u>   Signature: _____

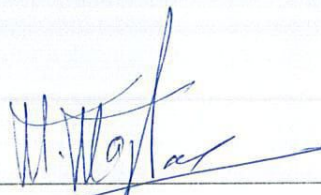_____
Head of Department

_____
Date

COUNTERSINGED

Date: <u>31|12|20.19</u>

_____
Dean/Principal

THESIS ACCEPTANCE CERTIFICATE

Certified that final copy of MS thesis written by **Ms. Naila Haroon,** (Registration No. **00000203210**), of **School of Natural Sciences** has been vetted by undersigned, found complete in all respects as per NUST statutes/regulations, is free of plagiarism, errors, and mistakes and is accepted as partial fulfillment for award of MS/M.Phil degree. It is further certified that necessary amendments as pointed out by GEC members and external examiner of the scholar have also been incorporated in the said thesis.

Signature: _____

Name of Supervisor: Prof. Muhammad Mazhar

Date: ___31–12–2019___

Signature (HoD): _____

Date: ___31/12/2019___

Signature (Dean/Principal): _____

Date: ___31/12/2019___

Dedicated to my lovely parents, respectable teachers, friends and my husband

ACKNOWLEDGEMENT

First of all, I present my humblest and earnest thanks to Almighty **Allah***, The Most Sympathetic and The Merciful, who blessed me with power to accomplish this project.*

I offer my sincerest gratitude to my supervisor, **Dr. Muhammad Mazhar***, who has supported me throughout my thesis with patience and knowledge whilst allowing me to work in my own way. I attribute the level of my Master's degree to their encouragement and effort.*

I would like to thankful to the members of GEC; **Dr. Manzar Sohail** *and* **Dr. Azhar Mahmood** *for their constructive criticism and suggestions for improvement. I greatly acknowledge the facilities and technical support provided by the other NUST schools like SCME and USPCASE.*

I would really like to extend my thanks to all the **lab staff** *for their assistance, my* **friends** *and grateful for their kind, friendly and moral support in my work as well as their company and cooperation during the times when I am encountered with difficulties.*

In the end, my humble is to my dear **parents** *who always prayed to* **Allah** *Almighty for my success and brought me with all her efforts. I would also like to pay my special tribune to my* **husband** *who encourage and supported me during all this period.*

Naila Haroon

Table of Contents

LIST OF FIGURES

LIST OF TABLES

LIST OF ABBREVIATIONS AND SYMBOLS

TPAOH	Tetrapropylammoniumhydroxide
AIP	Aluminium isopropoxide
TEOS	Tetra ethylorthosilicate
$Ni(NO_3)_2.6(H_2O)$	Nickel (II) nitrate
$Pd(NO_3)_2$	Palladium (II) nitrate
MOFs	Metal organic framework
PEC	Photoelectrochemical
SEM	Scanning electron microscopy
TEM	Transmission electron microscopy
EDS	Energy dispersive x-ray spectroscopy
BET	Brunauer-Emmett-Teller
XRD	X-ray diffraction
TGA	Thermogravimetric analysis
CA	Chronoamperometry
FTIR	Fourier Transform Infrared Spectroscopy
Rpm	Rate Per Minute
DFT	Density Functional Theory
DRS	Diffused reflectance spectroscopy
UV	Ultra Voilet region
Vis	Visible region

ABSTRACT

Zeolites due to their porous nature are called molecular sieves and have a lot of industrial applications. They are microporous, mesoporous and nanoporous materials which attract much attention due to their unique structural properties. Sodiumaluminosilicate decorated with Ni and Pd is synthesized by hydrothermal treatment at 120^0 C for 12 hrs. Molar ratio of the mixture, alkalinity, aging conditions, crystallization temperature and reaction time are important factors for the synthesis of mesoporous sodiumaluminosilicate. The material is characterized by Diffused reflectance spectroscopy (DRS), Fourier transform infrared spectroscopy (FTIR), X-ray diffraction (XRD), Thermogravimetric analysis (TG), Scanning electron microscopy (SEM), Energy dispersive spectroscopy (EDS), Transmission electron microscopy (TEM), X-ray photoelectron spectroscopy (XPS) and Brunauer-Emmett-Teller (BET). The UV-visible spectroscopy shows the absorbance edge at 260 nm and the band gap is 3.6 V calculated from tauc plot showing the efficient capturing of photons in UV and Vis region to generate electron and holes efficiently. IR bands at 670, 990, 1051, 1660 and 3375 cm-1 indicating Al-O bending vibration, Si-O-Si asymmetric stretching vibration, Al-O-Si asymmetric stretching vibration, H-O-H stretching vibration and OH groups of Si-OH stretching vibration respectively. XRD shows the peaks of support (aluminosilicate) only and the metal peaks are not detectable because of their addition in less amount. TGA shows no loss in mass. SEM/EDS shows layered structure having canals, pores and voids in between the layers with homogenously distributed nickel and palladium nanoparticles. TEM shows the presence of channels, pores and voids at various resolutions. The BET surface area is 875.178 m^2/g and Langmuir surface area is 1230.638 m^2/g. In this thesis, two aims are highlighted which are hydrogen storage and photoelectrochemical studies for water splitting. Due to its porous framework, hydrogen can be adsorbing in the voids of sodium aluminosilicate where metals are incorporated. The water splitting results are analyzed for Chronoamperometry (CA) and water stability are studied.

INTRODUCTION

1.1 Zeolites

Zeolites is a group of micro porous crystalline aluminosilicate which are largely used in industries due to their distinctive properties such as; greater stabilities, anionic frameworks and micro porous structures. These properties are intensely associated to the microscopic zeolite structures, which includes framework atoms and pore architecture. To control the zeolite microscopic structure, it is acute to comprehend the formation mechanisms of zeolite. Specifically, the interactions between aluminosilicate and structure directing agent are crucial to understand the mechanism of formation of zeolite. In hydrothermal method, OSDAs are introduced in crystalline zeolites cavities as molecules or cations. It is essential to improve molecular level of zeolite formation, having particular OSDAs parts by designing new zeolites with personalized chemical and structural properties. Zeolites are usually manufactured through hydrothermal methods from the reactants comprising a source of aluminum, a source of silicon, water having mineralizer and an OSDA. Synthesis of Zeolite is usually synthesized under high-temperature, highly alkaline, and at conditions of high-pressure, that mark the intermediate species characterization difficult in hydrothermal treatment. Additionally, there are numerous synthetic parameters (e.g., synthesis temperature, synthesis time, initial compounds and procedure of mixing) which are interdependent on each other, limit the whole zeolite crystallization considerate.

In spite of the above difficulties, several studies have traced the intermediates which are formed in crystallization of zeolite which is used to expose the connections between amorphous (alumino) silicate species and OSDAs. In recent times, the studies of molecular-level on the crystallization of zeolite have showed that zeolite crystallization does not obey the classical nucleation theory [1].

Sodium aluminosilicate gel is mostly hired for the synthesis of zeolites by numerous methods ranging from the simplest methods (i.e. hydrothermal method) to complex methods. Commercially synthesized zeolites are more frequently use than naturally synthesized zeolites because of their identical particle sizes and higher purity so, mark it more appropriate for most scientific purposes and engineering applications [2].

1.2 Description of zeolites structure

Zeolites have very sophisticated three-dimensionally stretched framework structures [3]. Zeolites are extremely crystal-like, porous aluminosilicate that is established on a 3-D complex linkage of tetrahedral $[SiO_4]^{4-}$ and $[Al_4]^{5-}$ and their skeleton is exposed structures having positive charge sited inside the pores of material. The positive charge counterbalances the anion on the frame. Xu et al. stated that the distinctive catalytic and ion-exchange properties of zeolites and further related materials is mainly the outcome of the movement of this positive charge. The word zeolite framework denotes a corner-sharing network of tetrahedrally synchronized atoms. Examples are: LTA [Linde zeolite A], MOR [mordenite topology], FAU [molecular sieves with a faujasite Topology], AFI [aluminophosphate AlPO4-5 topology], and MFI [silicalite topologies and ZSM-5]. Haranczyk and Zimmermann, Michalev and Petrov explain the zeolite structural formula that is founded on the crystallographic unit cell such as: $M_{x/n}$ [(AlO$_2$) x (SiO$_2$) $_y$] wH$_2$O, whereas the (M) denotes alkaline earth cation, (n) denotes valency of the positive charge, (w) denotes number of water molecules per unit cell, x and y denotes the total number of tetrahedra per unit cell [2].
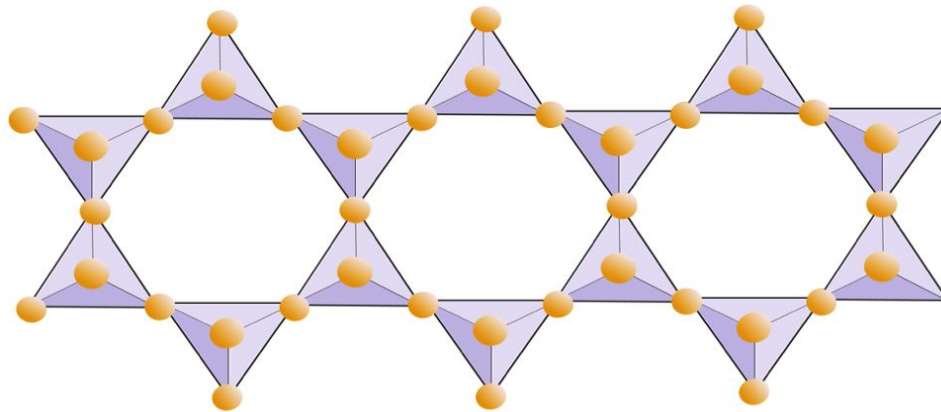
Figure 1: One-dimensional structure of aluminosilicate
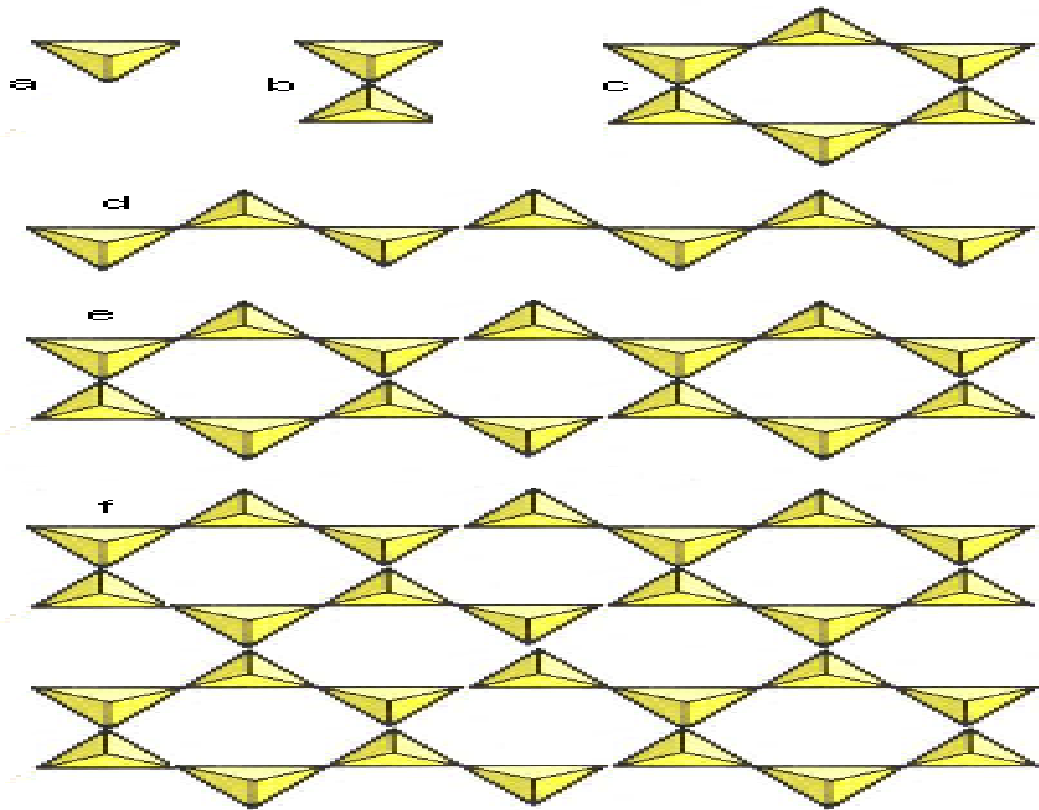
Figure 2: Three dimensional sheet like structure of aluminosilicate [4].
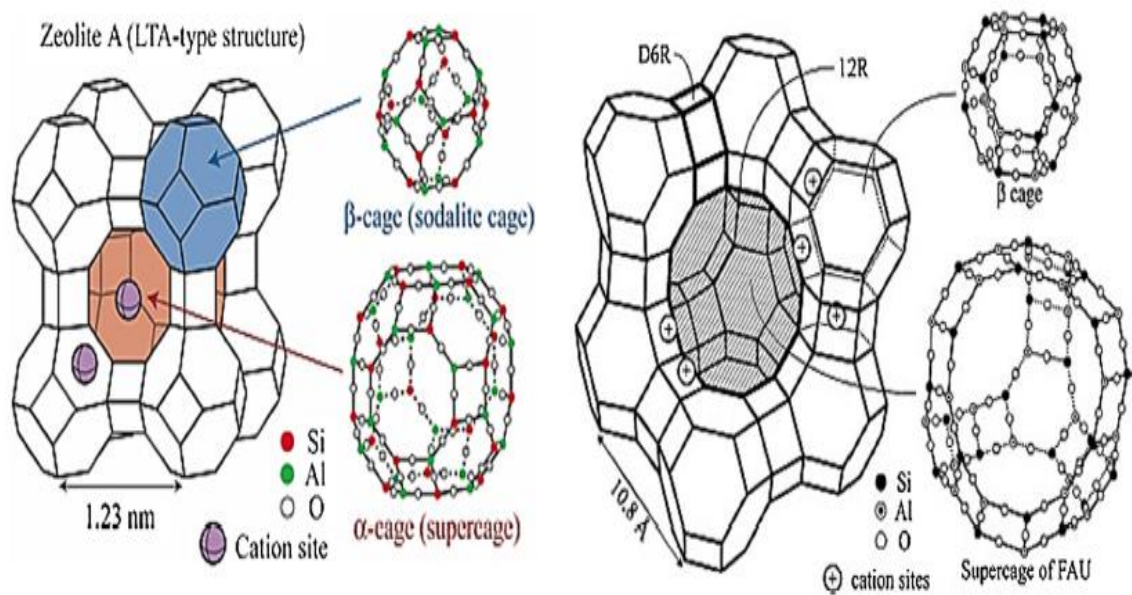
Figure 3: The structure of (a) LTA and (b) FAU type zeolite.

1.3 Zeolite synthesis by hydrothermal treatment

Zeolite synthesis by hydrothermal method is a multiphase reaction-crystallization procedure, generally incorporating and both crystalline solid and amorphous phases and at least one liquid phase. Yoshimura and Byrappa designated that the hydrothermal method is an in-situ reaction taking place beyond ambient temperature under pressure in an aqueous solution.

Usually zeolites (aluminosilicate) are synthesized through hydrothermal methods due to some benefits including low air pollution, high reactivity of reactants, formation of metastable phases low energy consumption, unique condensed phases, and easy to control the solution. Yet, Cox and Cundy retained that the hydrothermal process is the major synthesis path for many zeotypes and zeolite.
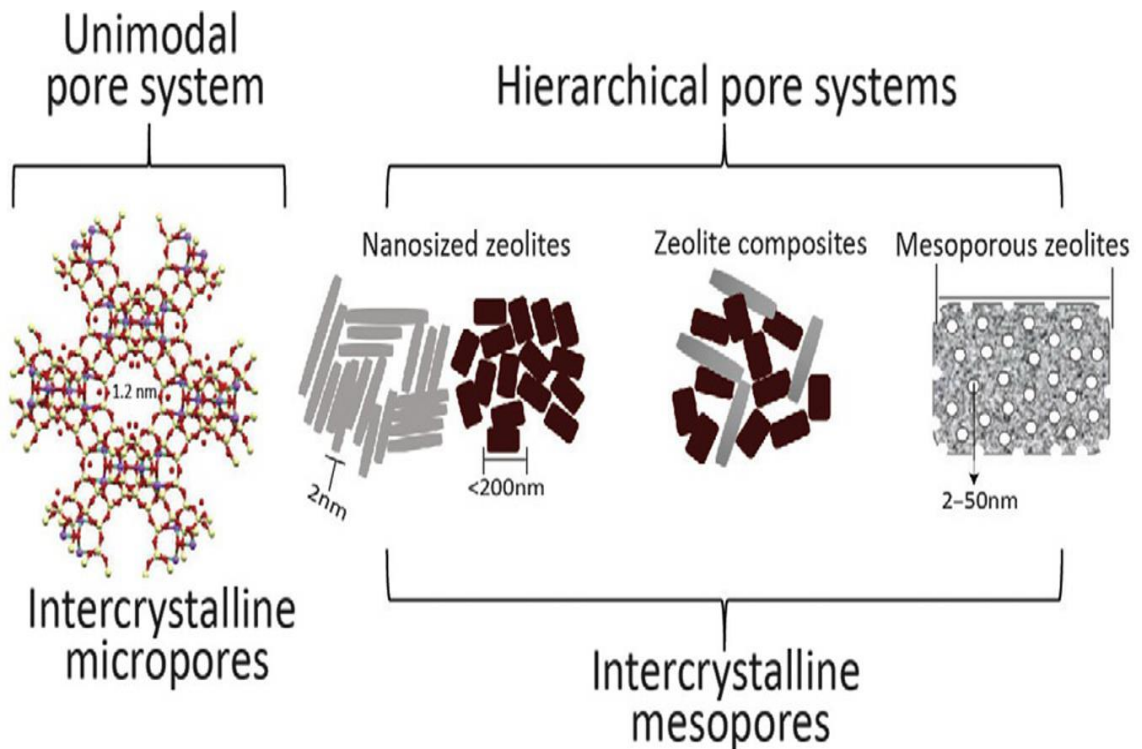
Figure 4: Characterization of zeolite materials with enhanced transport characteristics[5].

1.4 Chemistry of silicates

The silicates comprise two types: soluble and insoluble silicates.

1.4.1 Soluble silicates

The soluble silicates are derivative of alkali metals and they comprise variable amounts of water, silica and metal oxides. The compounds in this category are Na_4SiO_4 (orthosilicate), anhydrous Na_2SiO_3 (metasilicate), $Na_2Si_2O_5$ (disilicate), $Na_6Si_2O_7$ (pyrosilicate) and hydrates $Na_2SiO_3.nH_2O$ (n = 5, 6, 8, 9), $Na_2Si_4O_9.7H_2O$, $Na_3HSiO_4.5H_2O$. The soluble silicates are described by silica-to-alkali ratios up to 2 give true solutions however those having greater ratios provide colloidal solutions comprising distributed silicates. The soluble silicates are used to precipitate the metal salts solution, and the mixture of basic salts, hydroxides and silica instead of silicates forms the precipitates.

1.4.2 Insoluble silicates

The insoluble silicates are natural mineralized materials combine with definite synthetic zeolite-like compounds beneficial as an ion exchanger. These are complex series of materials when measured from the perspective of only chemical composition. Only the X-ray crystallography is applicable to study these type of materials and the systematic classification is only possible in relations of structural arrangements. These are the vital complications for silicates classification. Only the analytical data alone cannot predict the classification because a given data set for such complex materials might be reliable with such a large number of diverse molecular formulations. Moreover, the sample homogeneity and the consignment of any specific formula built upon analysis alone may be completely accidental. Isomorphous replacement is another factor in which ions such as Ca^+, Mg^+, Fe^+ etc. can substitute each other and analogous replacements comprising Na^+, K^+, and Al^+ or F^- and OH^- may take place in almost infinite variation. Such type of replacements doesn't implicate any change in general compositions or oxidation states, but they do enforce analytical problems.

The most important sort of replacement is silicon by aluminum. This is feasible due to size similarities ($rSi^{+4} = 0.50$ A, $r_{Al}^{+3} = 0.55$A) and is very common. Due to the variances in oxidation number, exchange of silicon by aluminum increases the oxidation state of anion by one unit and needs the occurrence of either a balancing positive charge (e.g.,

Na$^+$) or an additional isomorphous replacement of one positive charge by another higher cation (e.g. Na$^+$ by Ca$^+$). As silicon is all the time 4-coordinate to oxygen and aluminum might be 4-coordinated or 6-coordinated. As an AlO$_4$ group should be the structural correspondent of a SiO$_4$ group, however an AlO$_4$ group would not. Apparently, the only rational classification of silicates is based upon their structures [6].

1.5 Applications of zeolite

Commercially, zeolites are working in adsorption (separation), ion-exchange and catalysis applications. Mostly, catalytic usages are exploited in environmental technology and hydrocarbon (refining, petro chemistry), whereas sorption and ion-exchange are found in desiccants/adsorbents and detergent powders of laundry. Mesoporous zeolites have found commercial applications with the arrival of MCM-22 (MWW), ZSM-5 (MFI), ferrierite (FER), e.g. in ethyl benzene synthesis (MWW), xylene isomerization or refinery dewaxing (MFI), and olefin isomerization (FER). Majority of these hydrocarbon processes depend on selective effects of shapes inside their specific voids [7].

Currently, environment and energy have turn out to be crucial worldwide issues for ecological enlargement of industries (chemical and petrochemical) and zeolite materials plays significant roles to report it. These are applicable for catalytic conversion processes due to taking part of zeolite materials with high selectivity and activity that extensively rise the atomic economy of the procedure by improving the target product's yield [8].

1.6 Organic structure-directing agents (OSDAs)

Organic structure-directing agents (OSDAs) are frequently used for the zeolites synthesis, particularly silicon-to- aluminum of high ratios. Moreover, numerous zeolites having unusual new structures or chemical composition are designed by using numerous identified OSDAs.

These types of OSDAs are usually sealed in the voids of zeolite as an inaccessible molecule or cation. The illustrative specimen is the tetrapropylammonium (TPA+) cation situated at the intersection of zeolite channel. The route of structure of these OSDAs described in the form of a geometric fitting among zeolite cavities and isolated OSDAs

which leads to the maximum stabilization energy that is computationally predicted in the siliceous zeolites.

Though, the zeolites (aluminosilicate) formation is very difficult and kinetically organized so there is no need to the formation of the utmost stable crystalline phase. thus The interpretation of the OSDAs structure direction can add to the systematic and rational exploration for zeolites having distinctive structures and extra-large pores [9].
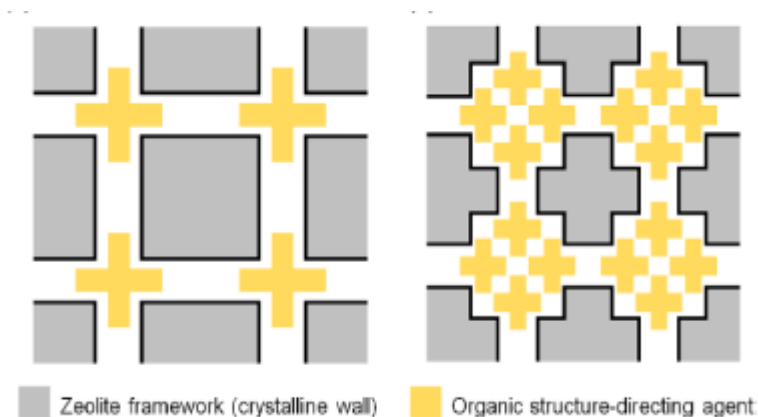
Figure 5: Schematic diagram of structure direction in (a) isolated mode (b) clustered modes.

1.7 Encapsulation of metals

The applications of zeolites utilize the shape-selective and molecular sieving properties, which lead to entrance regions of intracrystalline by particular molecules, that is founded on the shape and size of the joining cavities and openings contained by individual porous framework. In particular, catalysts of Zeolite get advantage from the omission of enormous poison or reactive molecules from the active sites of intracrystalline, from the retaining of huge products till they splinter and exit more eagerly as slighter sort of species, and also from the favored steadiness of particular transition states inside intracrystalline spaces as well. These properties are able to be joined to the intrinsic catalytic properties of metal surfaces through metals encapsulation inside the spaces of zeolite therefore, shape-selective and size-selective metal catalysts can be synthesized.

Mostly noble metals like Pd, Pt, Rh, Ir, Re, Au, Ag, as well as their bimetallic mixtures are effectively encapsulated in numerous zeolites (e.g., FAU, LTA, CHA, MFI). The

successive reduction of these metals and the Ion exchange of metal cations by H2 facilitate encapsulation in large-pore zeolites (12-member ring (MR) openings or larger; e.g., FAU). These type of approaches are inappropriate for small-pore zeolites (8 MR) and, in few cases, for medium-pore zeolites (10 MR) as well due to the gentle diffusion of solvated aqueous precursors via their slender openings. The encapsulation of the base metals (e.g., Pd, Fe, Ni, and Co) and their oxides has too noteworthy importance due to their abundant usage as catalysts. PdO, Fe_2O_3, Co_3O_4, and NiO are operative oxidation catalysts for various substrates, like methane, CO and alcohols. These oxides are able to reduce into their metallic state to make them advantageous catalysts for hydrogen storage (Ni, Pd), hydrocarbon reforming (Ni), ammonia synthesis (Fe), Fischer- Tropsch synthesis (Fe, Co) and aldehyde hydrogenation (Ni).

Pd^{+2}, $Fe^{2+,}$ Co^{2+} and Ni^{+2} cations are able to swapped from the aqueous media on most of the zeolites as they can diffuse in their divalent state even through the 8-MR zeolite openings. However, the transformation of these swapped positive charges into clusters of metals by post-exchange reduction in CO or H_2 but generally, cannot utilize to form encapsulated base metals due to higher temperatures necessary for their reduction (>727 ^0C) which lead to structural breakdown and agglomeration of their crystalline microporous frameworks. Actually, such temperatures transform crystalline aluminosilicates into refractory metal aluminosilicates (e.g. $CoAl_2O_4$) or huge particles of metal at the sites of extra crystalline and amorphous mesoporous solids.

Generally, the procedures which have been described for effective encapsulation of Pd, Co, Fe and Ni oxide clusters in MFI, FAU and LTA provide administrative principles and definite protocols which in general can be smeared to the systems of zeolite-metal and the system-specific encapsulation of Co_3O_4 bunches in LTA that have been described formerly [10].

1.8 Hydrogen storage concept

Currently, fuel cell vehicles, sold and manufactured through several different companies like Hyundai, Honda and Toyota. They practice 70 MPa compacted hydrogen storage which is quickly fetching the customary of industry. By storing hydrogen at this pressure requires costly cylinder-shaped carbon fiber fused tanks. Significant energetic expenses

together with geometrical restrictions and economic costs are related with compressing hydrogen and supplying to storing tank. During quick filling, thermal effects from isenthalpic expansion mean that hydrogen need to be precooled at about -40^0 C to avoid overheating, that additionally rises the energy consequences that is related by using hydrogen at high pressure. Thus emerging low pressure, low cost substitutive methods for storing hydrogen remains aim for long term.

Physisorptionaly storing hydrogen in higher surface area nanoporous materials at low pressures with adsorbents likewise Metal-Organic Frameworks (MOFs) displays significant potential in this respect.in comparison to utmost other solid state storing methods, hydrogen physiosorption is also fast and fully reversible and in comparison to chemisorption, it has small enthalpy of adsorption which decreases thermal management problems such as storing hydrogen in complex hydrides.

Specific approaches to enhance the storing capacities of nanoporous materials which includes useable, volumetric, and gravimetric capacities whereas the exploration of new hydrogen storing materials via machine learning. New materials will prove operative in future for hydrogen storage through physiosorption.
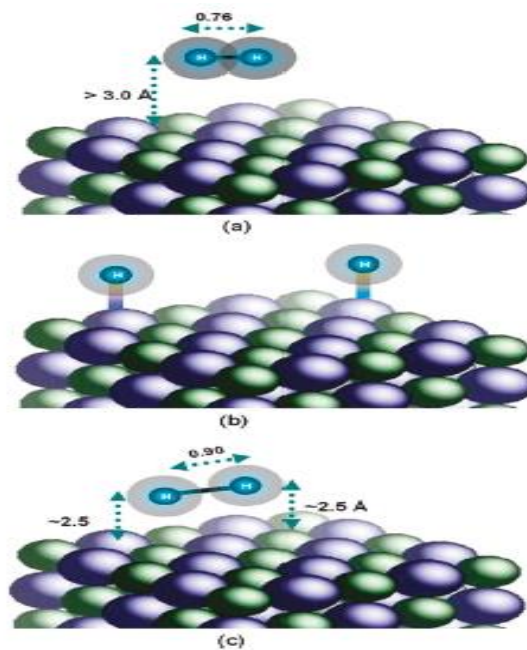
Figure 6: Hydrogen adsorption on substrates (a) physiosorption (b) chemisorption and (c) quasi-molecular bonding.

1.9 Hydrogen storage materials and their limitations
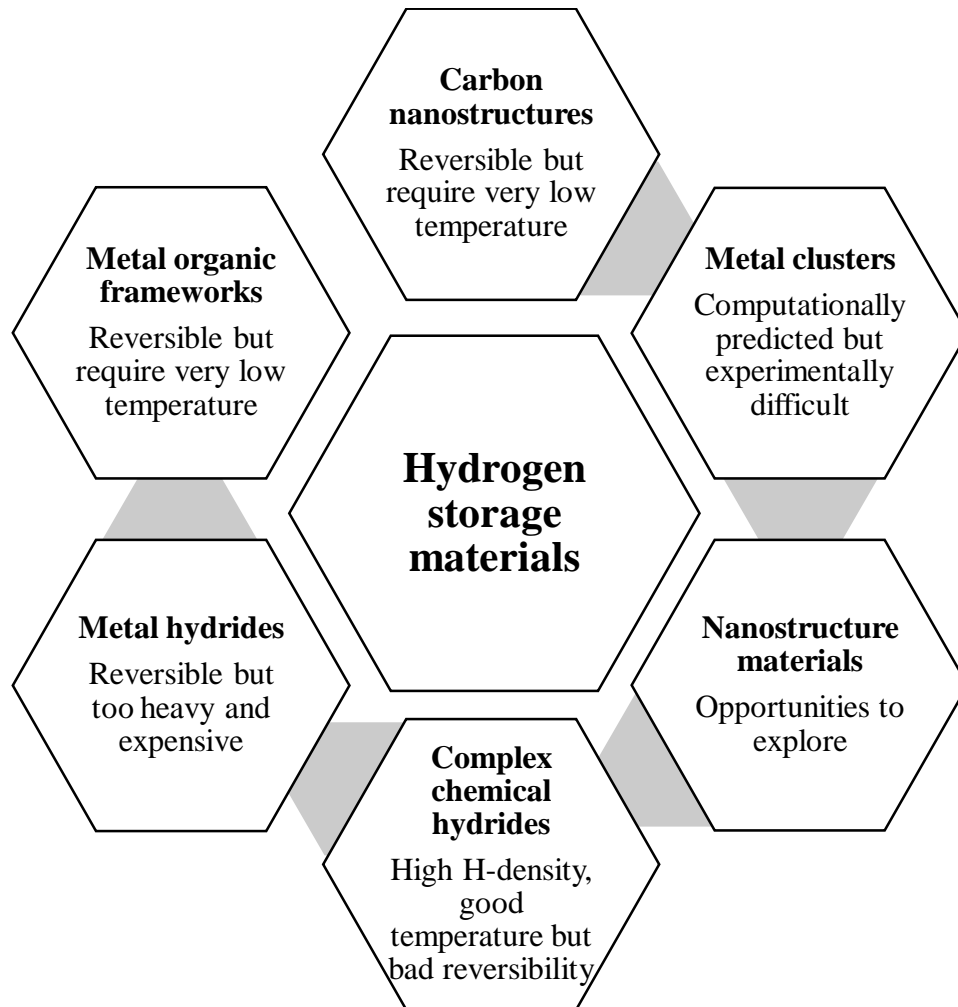
Figure 7: Summary of various hydrogen storage materials and their limitations (figure adapted from a talk given by Professor W.I.F. David of Oxford University)

1.9.1 Gravimetrical capacity

Gravimetric capacity is the amount of H_2 adsorbed per unit mass, expressed as kg H_2 kg^{-1}, for example, weight percentage (wt.%) is significant as hydrogen own a very little molar mass.

The sort of a hydrogen fuel cell vehicle will be restricted if a storing reservoir having the stuff, weighs the most.

This is a problem with lengthier driving series, organized with much smaller refueling times, is the most important benefit of hydrogen fuel cell vehicles associated with their

electronic battery counterparts. A Chahine's rule (enhancing gravimetric capacity with enhancing surface area) perceived for the nanoporous materials, which includes MOFs, porous carbons, and numerous other materials. This empirical relationship proposes that, at higher pressures (~3.5 MPa) and temperatures 77 K, almost 1 wt% acceptance is attained for every surface area of 500 m^2g^{-1}. As per Chahine's rule, high surface area would lead to larger gravimetric hydrogen uptakes.

Therefore, accounts of predominantly higher BET areas are essentially preserved with certain cautions. Moreover, materials having high BET areas owing wide pores, for example their exposed frameworks inhabit a lesser amount of bulk volume of material with growing surface area.

Goldsmith et al. determined, in 2013, that "Storing H_2 in MOFs will not help from further progresses in surface area alone."

1.9.2   Volumetrical capacity

Gravimetric capacity controls the storing reservoir weight essential to store a known quantity of H_2 as well as volumetric capacity controls the container volume and it is defined as the amount of H_2 adsorbed per unit volume, for example, as g H_2 L^{-1}. Therefore, computing the material volumetric capacity needs the understanding of its density or bulk volume. Packing density is the more accurate definition for both amorphous and crystalline materials whereas the packing density may be attained from bulk volume which is employed by the compact or a monolith external volume, or sample of powder particles or small crystallites, these all are dependent on the type of adsorbent. The volumetric capacity increases by increasing the volumetric surface area (surface area per unit area in units of m^2 cm^{-3} or m^{-2} mL^{-1}).

Different methodologies adopted to increase surface area volumetrically. The occupied volume can be decreased by using compression. The samples that is produced as powders comprising crystallites or small particles can be molded into monoliths which own a greater bulk density as compared to loose powder. The alternate for MOFs is the usage of interpenetration which reduces pore size and enhances the volumetric surface area of the single crystal.

Crystalline materials like MOFs are generally manufactured as powders, whose bulk density is quite low. Powders are able to be compressed which enhance their volumetric H_2 storing capacity and bulk density. This has verified for large number of materials such as MIL-101, MOF-177, and MOF-5. Zacharia et al. studied that by compression of MOF-177 is able to enhance surplus H_2 capacity up to 80% in comparison to the powder MOF-177. By increasing the bulk density, H_2 storing capacity decreases because of the pores collapsing.

1.9.3 Useable capacity

Most frequently, Hydrogen storing capacities are stated in the form of absolute, maximum excess or total uptake at high pressure. Basically, the most important factor is the useable capacity which is also known as deliverable or simply the delivery or working capacity in terms of pressure and temperature under filled tank conditions and that of the capacity under exhausted tank conditions.

The useable capacity works as a purpose of temperature for inflexible materials displays a maximum that describes the optimal working temperature which is greater for those materials having a greater adsorption enthalpy. High enthalpy enhances that temperature at which H_2 is adsorbed but attaining a high value only at low coverages cannot rise the useable capacity because H_2 confined on the sites of high energy. Lower enthalpy lowers the H_2 amount confined at lower pressure and enhances the useable capacity at a specific temperature for any known pressure.

Enlightening hydrogen storing in nanoporous materials essentially be deliberated while emerging and manufacturing novel materials and recognizing novel compounds as possible Hydrogen storing materials. Numerous types of porous materials have been revealed in which many materials have not yet been explored for hydrogen storing applications.

New class is nanoporous molecular crystals have appeared having porous organic cages as auspicious aspirants for applied uses. Porous organic cages have comparatively lower gravimetric surface areas as compared to PAF-1 and MOFs. Recently, compound of boronate ester having BET area above 3700 m^2/g has testified.

In comparison to frameworks (like COFs, PAFs and MOFs), nanoporous molecular crystals contains distinct molecules which are formed by crystallization. These distinct molecules are linked by weak molecular interactions i.e. hydrogen bonds or van der Waals forces. It permits development of co-crystals, comprising two or more dissimilar types of cage. This deals with merging the properties of dissimilar compounds and offer unique and fascinating functionality. Vital differences between these framework materials and solids also comprises stimulating opportunities for functionalization. Amorphous molecular solids can also be made, having sorption properties which vary from their crystalline complements, whereas manufacturing of core-shell particles can also be imaginable.

As renowned earlier, that the interactions in H_2 storing material is significant in defining H_2 storing properties of a material. Such interactions can be enhanced by modifying materials through the introduction of metals open spots or functional groups in case of MOFs. Generally, the strength of H_2-metal interactions is influenced by the type of metal atom [11].

1.10 Photoelectrochemical splitting of water

Through the use of solar energy, production of hydrogen is carried out through photoelectrochemical (PEC) water splitting. Due to direct sunlight usage, production of hydrogen makes this method cost effective, renewable and environment friendly [12]. The conventional PEC cell consists three electrodes (a semiconducting working electrode as photcatalyst, a reference and a counter electrode) which are submerged in an electrolyte. The absorption of photons excites working electrode to create charge carriers, holes and electrons. In a usual PEC cell, holes contribute in the oxidation reaction and electrons contribute in reduction reaction. OER is taking place at the interface of electrolyte/semiconductor leads to the production of oxygen gas and Hydrogen evolution reaction, HER is taking place on the counter electrode in the presence of electrocatalyst leads to the production of molecular hydrogen [13,14].

1.10.1 Properties of semiconducting photo electrode

There are following properties of a semiconducting photo electrode for efficient PEC water splitting which are:

a) Outstanding characteristics of solar absorption
b) Prompt separation of charge carrier
c) Alignment of band edge with redox level of water for oxidation/reduction of water
d) Available in abundance
e) Cost-effective
f) Stable photochemically

Though, such type of semiconductors is not known yet which have all these properties. So the main thing is the finding of such semiconductor for effective PEC water splitting which have most of the above properties and which can absorb sufficient solar energy for driving the water splitting effectively [15].
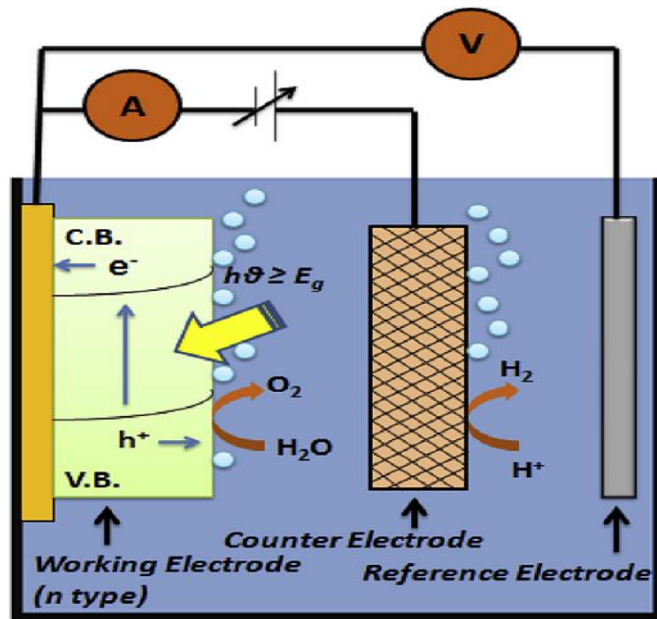
Figure 8: A conventional PEC cell

Generally, water splitting in sunlight has gained a lot of devotions for production of renewable hydrogen from water on a huge measure [16-18]. Solar hydrogen will perform a significant role in the sustainable-energy cultures for the reason that it is transportable, storable, and can be transformed efficiently into electricity by consuming fuel cells when

it will be essential. Furthermore, hydrogen is appropriate in the present chemical industry as feedstock and can be used for carbon dioxide recycling by means of chemical methods such as the methanol synthesis and Fischer–Tropsch reaction. As the reaction of water splitting is a demanding reaction where Gibbs free energy rises by 237 kJ mol^{-1}. The energy is delivered through light or ideal sunlight which is required to drive PEC water splitting and photocatalytic. Fig 9. displays the graphic representation of photocatalytic water splitting reaction process.

Holes and Electrons are produced in semiconductor photocatalyst particles through the excitation of band-gap. Photoexcited carriers are shifted to active sites of the surface and successively used up by reduction-oxidation reactions of the surface. Diffusion of mass for reactants and products would continue parallel and the recombination of photoexcited carriers happens beside these reactions. So, for effective water splitting, the charge separation in redox reactions and photocatalyst particles on their surfaces should carry on lifetimes. In several cases, recombination is the chief process which photoexcited carriers must endure. photoelectrodes and photocatalyst are amended with suitable buffer layers and cocatalysts to assist surface reaction and charge separation.

Current progresses in PEC water splitting and photocatalytic in visible light are defined in the perspective of reaction conditions, loading of co-catalyst, electrode fabrication processes and surface modifications [19]. A lot of informative articles on the production of solar hydrogen have been issued, presenting reaction systems of reaction [20,21], selected promising materials [22], extensive material development [23,24,25], nanostructuring [26], and kinetic aspects [27].
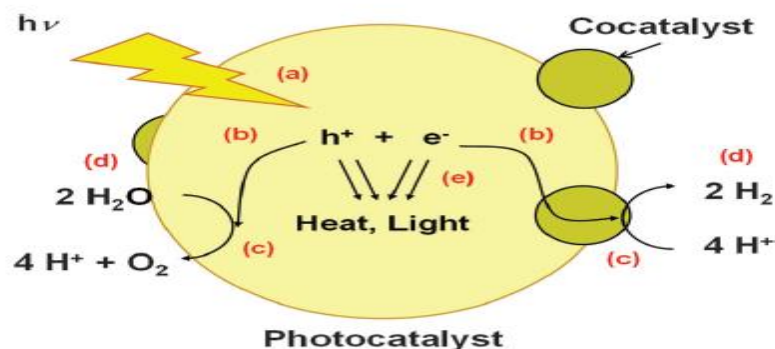
Figure 9: Water splitting process on a heterogeneous photocatalyst (a) absorption of light (b) transfer of charge (c) redox reactions (d) adsorption, mass diffusion and desorption of chemical species (e) recombination of charge

1.10.2 Z-scheme water splitting

A sequence of electron transfers processes step by step to generate adequate energy for water splitting and as a result, light reaction of natural photosynthesis take place so this process is called Z-scheme [28].

Generally, water splitting has succeeded with roughly single nonoxide photocatalysts. Though, the active photocatalysts absorption wavelength was 500 nm, that was very short to gather sunlight successfully. Z-scheme water splitting is beneficial in a wide range of visible light, as semiconductors by the use of either water reduction or oxidation potentials.

In Z-scheme water splitting, $BiVO_4$ and WO_3 are used as photocatalysts of oxygen evolution. Additionally, $BaTaO_2N$, having absorption edge wavelength is 660 nm, is used as photocatalyst hydrogen evolution. The photons number are necessary to produce hydrogen is double to that of which is essential for one-step splitting.

Moreover, the Z-scheme needs a well-adjusted photocatalytic activity of the photocatalysts oxygen and hydrogen evolution in a suitable redox facilitator concentrations and pH conditions. It is acute to overturn backward reactions relating redox mediators which are thermodynamically favorable as compared to water splitting in Z-scheme water splitting. The forward reactions would progress proficiently to escape any side reactions.
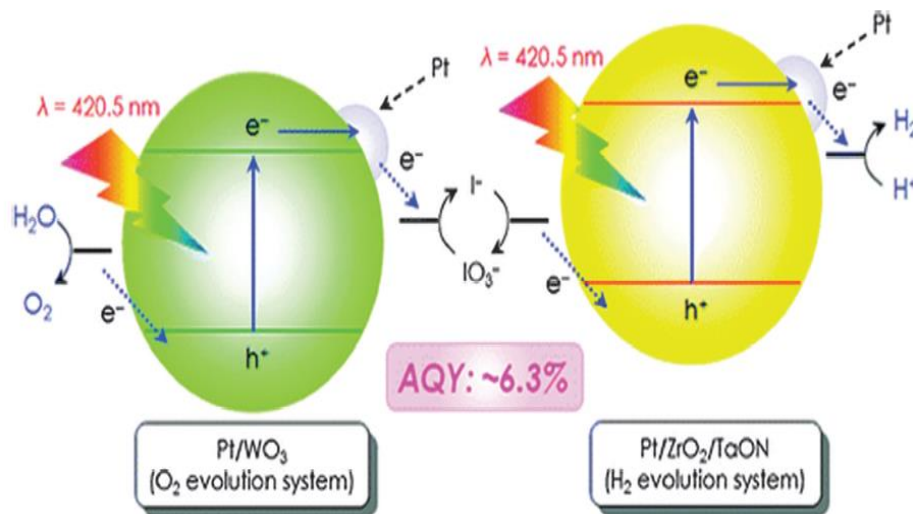
Figure 10: Z-scheme schematic reaction for water splitting by using Pt/WO3, IO3-/I- and Pt/ZrO2/TaON

Z-scheme water splitting through interparticle electron transfer is beneficial over conventional Z-scheme water splitting along with reversible reduction-oxidation couples in the thermodynamically favorable backward reactions relating reversible reduction-oxidation couples do not occur [19].

1.11 Characterization techniques

1.11.1 Infrared Spectroscopy

Infrared Spectroscopy (IR) is suitable for organic compounds identification. IR can be accomplished on the samples as minor as 10 mm by the usage of a specialized microscope. It is a significant micro analytical technique. Bonds of Molecules vibrate at distinguishing frequencies. If the vibrations of a particular molecule bring about an alteration in the dipole moment of the bond, then that molecule is capable to absorb IR radiations of that distinguishing frequency. The sample is illuminated by a broad band of infrared frequencies, and the strength of transmitted or reflected infrared radiation is measured as a frequency function. The spectrum of infrared absorbance can be remodeled through the understanding of transmitted/reflected intensity and incident intensity. At particular frequencies, Absorption is the distinctive of sure bonds. Hence, the IR spectrum recognizes various functional groups and bonds inside the molecule. Moreover, massive libraries of spectra of IR also help to recognize unknown compounds or help them to place into certain categories of molecules [29].

Information about the samples functional groups can be founded by absorption band frequency when compared to standard spectrum [30]. The IR spectroscopy is the technique of spectroscopy which deals with infrared region. The electromagnetic spectrum of the IR portion is divided into three regions: The near region (14,000–4000 cm^{-1}) gives the information of the harmonic or overtones vibrations related to the tensions of hydrogen. The central region (4000–400 cm^{-1}) where the rotational-vibrational structure and fundamental vibrations are studied. The distant region (400–10 cm^{-1}) gives evidence from vibrations of crystal lattice, rotational transitions, and the molecule skeleton [31].

1.11.2 X-Ray Diffraction Spectroscopy

X-ray diffraction (XRD) is a typical method for recognizing the chemical structures of organic and inorganic crystalline materials. Beams of X-ray which invade on a commonly ordered lattices go through destructive and constructive interference, which depends on the X-rays wavelength, the lattice spacing's, and the angle of incidence of the beam of X-ray. When the sample rotates comparative to a static source of X-ray, there are certain variations occur in interference which leads to distinguishing diffraction patterns. By comparing these patterns of diffraction with reference spectra, identification of specific crystalline phase take place. Amorphous materials cannot generate diffraction pattern [29].

The profile of XRD diagram offers a knowledge of the degree of order/disorder about the given structure. X-Ray diffractometer (XRD) was applied on sodium aluminosilicate decorated with Ni-Pd with 2θ range between 10^0 and 90^0 in this context [30].

1.11.3 Thermal analysis

Thermal analysis is a technique where DTA/TGA curvatures are used as the finger print of material. In a usual thermogram of TGA, the schemes first display weight loss analogous to the removal of moisture by heating the material from 25 to 150 °C. In the next step (150–400 °C), there is the maximum weight loss, analogous to active pyrolysis or primary carbonization, is the result of elimination of volatile materials etc. This step is separated into two portions analogous to breakdown of hemicelluloses (180–270 °C) and celluloses (270–400 °C) [33-36]. In the next third step (400–550 °C), there is a display of the breakdown of structure by higher stability [34]. Beyond 550 °C, there is a minor weight loss. Beyond 550 °C, there is a minor mass loss and becomes nearly constant.

The thermogram of DTA is somewhat alike to the thermogram of TGA. In the DTA, temperature of testing sample is measured comparative to the nearby inert material [37]. Usually, two peaks can be recognized separately for the heat treatment of biomass in an inert air. The first step is allotted to thermal breakdown of hemicellulose whereas the second step is allotted for the breakdown of lignin and cellulose. Usually, the second peak

includes longer range of temperature. Mostly, these two peaks overlap for several precursors of biomass [30].

1.11.4 Scanning electron microscopy (SEM)

Scanning electron microscopy (SEM) provides the magnifications of images up to 100,000 by a conservative thermal filament source or 1,000,000 by a field emission source. The magnificently absorbed beam of electron is skimmed on the material in SEM. The contact of energetic incident beam of electrons with the sample generates secondary electrons, X-rays and backscattered electrons. When the flux of any of these particles types are measured as a function of scan position then a map or an image of sample is displayed and reconstructed. Each particle type delivers diverse evidence about the sample hence, suggests dissimilar contrast mechanisms.

For example, secondary electrons convey evidence about topology of sample. Backscattered electrons convey evidence about average atomic number of the area [29]. Scanning electron microscopy (SEM) micrographs normally show modifications in the morphology of the materials. Images of Transmission Electron Microscopy (TEM) offer a comprehensive explanation of the classic, novel crystalline and disorderly samples [30].

1.11.5 Energy- Dispersive X-Ray Spectroscopy (EDS)

The analysis of EDS is used to accomplish spot chemical analysis or elemental maps by applying characteristic x-rays produced from the material. The X-rays are produced through the inelastic collision between higher energy incident electron and the electron located in the discrete orbital of atom within the sample which jumps to the lower energy state due to de excitation, generating x-rays having fixed wavelength that depends on the difference in energy levels of electron in different shells for the given element, so each element which is "excited" by the beam of electron, yield characteristic x-ray. Hence these x-rays which are produced from various dissimilar elements are gathered by the particular detector, which measures its energy and compared to the standard elements that are used to discover different elements in the desired material.

Alongside to the qualitative analysis, elements can be measured quantitatively merely by means of calculating counts at the specific energies [32].

1.11.6 Transmission electron microscopy (TEM)

Transmission electron microscopy is a technique which used highly energetic beam of electrons that is transmitted via extremely thin sample (~100 nm thickness). TEM is highly magnified than SEM (up to several million times). By using extremely thin sample, TEM image is extremely fine. Transmission electrons go through the diffraction effects that can be used to define phases of crystal in material just like XRD [30].

1.11.7 X-ray photoelectron spectroscopy(XPS)

For the chemical analysis, the XPS is an advent technique used for the characterization of powder and solids materials because of the measurement of variations in binding-energy which results from their chemical environment. Each electron's kinetic energy is related to the emission electron's orbital energy, and the orbital energy is the distinctive characteristic of molecules or atoms. The samples chemical composition containing light elements like oxygen, carbon, nitrogen and hydrogen are obtained through XPS. As XPS is a method of surface analysis so the depth of the materials should be less than 5 nm [30].

1.11.8 Brunauner, Emmett and Teller (BET)

For surface area calculation, the BET concept, established by Brunauner, Emmett and Teller. It is the most prevalent method for calculation of surface area of the porous solids. However, the practice of standard isotherms (isotherm data for the distinctive system of adsorbate–adsorbent) is quiet extensively used.

So, the specific surface area (S_{BET}), that is intended by BET technique, the relative pressure (0.05 to 0.25) is used to escape miscalculation of the specific surface area. The total pore volume is determined at the relative pressure $p/p_0 = 0.99$. Meanwhile, the conservative comparison from the α_s and t plots that is founded on N_2 adsorption for non–porous carbon as a reference also provides important evidence. The α_s method, that is resulting from the alteration of the method of t-plot is used to estimate an experimental isotherm from a standard isotherm which is used as a reference data. The use of the standard method of α_s and its extension lead to high resolution isotherms permits the

calculation of different textural parameters like the total surface area (S_{tot}), non-microporous surface or external surface (S_e), and a micropore volume (V_{mi}).

The classification agreeing to IUPAC the distribution of pore size is: macropores (> 50 nm), mesopores (2–5 nm) and micropores (< 2 nm). Moreover, the micropores are separated into narrow (< 0.7 nm) and wide (0.7 nm) pores. Thus, the PSD comprehensive explanation is used to predict and identify their performance for evolving novel materials and industrial applications [30].

1.11.9 Chronoamperometry (CA)

Chronoamperometry is a time-dependent technique which is dependent on time. In CA, a square-wave potential is put on the working electrode. The current of electrode, measured as a function of time, oscillates conforming to the analyte diffusion from the immense solution in the direction of surface of sensor. Therefore, Chronoamperometry is used to measure time-current dependence for controlled process of diffusion that is taking place on the electrode. It fluctuates with the concentration of analyte. Chronoamperometry is a susceptible method that does not involve tagging of the bioreceptor or analyte and it has been smeared independently or with other techniques of electrochemistry like CV in several studies [38].

1.12 Aims and Objectives

i.   To synthesize Nickel and Palladium decorated sodium aluminosilicate by hydrothermal method

ii. To carry out Hydrogen storage activity by using the metals Nickel(Ni) and Palladium(Pd) decorated on sodium aluminosilicate

iii. To carry out photoelectrochemical(PEC) water splitting study

LITERATURE REVIEW

H.Wang et al. studied that the higher capacity hydrogen storage is a crucial problem for hydrogen energy in future. The hydrides consisting light weight elements like Al, Li, Si, C, B, Mg, Na, N, etc. are best aspirants for high volumetric and gravimetric capacity of hydrogen storing. Though, the hydrides having light weight elements usually undergo poor reversibility at adequate pressure and temperature conditions because of excess high thermodynamic stability. Latest advances in the overcoming of kinetic and thermodynamic trials for complex hydrides and hydrides based on Mg. With respect to the enhancement of kinetic, countless accomplishments have been attained via numerous fruitful methodologies like catalyzing, compositing and nanoscaling. In specific, a massive and simple fabrication technique was established to in-situ form multi-valence nano-catalyst in hydrides based on Mg by conservative hydrogenation treatment and melting. The complex hydrides reversibility can be significantly enhanced via doping catalysts and nanoscaling. Relatively, the destabilization effect of thermodynamic is restricted by smearing the tactics of ionic substituting for complex hydrides, altering the reaction route, nanoscaling and alloying for Mg based hydrides.

To obtain nanoscaling, both experimental results and theoretical calculations verify that the destabilization of thermodynamic can only be attained by decreasing the hydrides size up to several nanometers that is tremendously problematic to maintain and realize so, nano-confinement has been implemented. Moreover, the reversibility of utmost alloys based on Mg is usually deprived, and fully reversible hydriding has been attained in some solid solution alloys based on Mg with low enthalpy of reaction. Based on the recent progresses in research, the existing complex and Mg based hydrides could not completely fulfill the application desires of hydrogen energy storage, and the maintainable research struggle are still building to resolve their intrinsic kinetic and thermodynamic tasks [39].

H. Barthelemy et al. studied that effective storing of hydrogen is critical for the victory of markets of hydrogen energy (primary markets along with the market of transportation). Hydrogen can be deposited either as a refrigerated liquefied gas, cryo-compressed gas,

compressed gas or hydrides. Compressed and cryogenic storage are the best advanced technologies for hydrogen storing. Applications of hydrogen energy activated the progress of high pressure compressed storage in mixtures pressure containers and novel solutions such as hydrides and cryo-compressed.

The possibility of those former technologies has been verified whereas the regulation and standardization agenda is in the process of manufacturing. Magnesium hydride is one of the supreme auspicious aspirants for solid-state hydrogen storage. As regards of composites pressure containers, tasks remain to progress the reliability and durability while still making sure the welfare of containers in service above 20 years and further for high pressure storing (up to 70 MPa). In specific, the influence of working settings on the structure and materials has assessed to upgrade the selection of materials, operating conditions and qualification tests whenever needed. Periodic examination tools have also established to estimate if the composite overwrapped pressure vessels quiet turns for facility [40].

E.B.G. Johnson et al. studied that numerous zeolite types established which were based on kaolinite in last years. Information's about zeolites based on kaolinite and the significant factors in their synthesis were focused. The effects of metakaolinization temperature and time, SiO_2/Al_2O_3 (Si/Al) molar ratio of the gel mixture, alkalinity, aging condition, crystallization temperature and time are some of the factors which were discussed.

In the hydrothermal treatment of zeolites based on koalinite, stirring at room temperature for 48 h is appropriate for several zeolites types and metakaolinization at 600 to 700 °C, whereas the time of 2 h is sufficient to convert the kaolinite into an amorphous type. Though, there are numerous vital aspects that should be deliberated to yield particular zeolites. Low molar ratio of Si/Al (Si/Al ≤ 5) yields SAPOs, X zeolites and various LTA types.

Whereas high molar ratio of Si/Al (Si/Al ≥ 5) yields ZSM-5, various types of zeolite Y, and zeolites beta. Concentration of NaOH ≤3 M is most appropriate for zeolite as greater concentration decreases the comparative crystallinity and yield hydroxysodalite as contaminations. Temperature of Crystallization should be ≥70 °C and ≤200 °C, because

if the temperature will be ≤70 °C then it will not sufficient for the synthesis of crystalline species. As the crystallinity rises with time. Though, crystallization time of 24 to 120 h is sufficient for zeolites synthesis [41].

Tijjani Abdullahi et al. studied that through hydrothermal process, synthesis of zeolite has been generally used for periods. Though, the severe terms of sustainability that indicates towards waste reduction, costs reduction, excluding adverse environmental influences and enhancement of proficiency of several system does not fulfill. The current developments in the zeolite synthesis through hydrothermal treatment, devotion is remunerated to the manufacturing raw materials which is in the form of wastes and consumption of natural resources for the synthesis of zeolite. For sustainable zeolites synthesis through hydrothermal treatment from kaolinite natural resources, optimal conditions are also considered. The conventional synthesis of zeolites that pays pure sodium aluminate and sodium silicate are costly, have adverse influence on the environment in comparison to the zeolites synthesis which is founded on kaolinite. For optimal specific zeolites synthesis by using kaolinite, the elimination of contaminations by consuming dispersant agent preceding to calcination from raw clay is significant, whereas the temperature of calcination is designated into three phases:

Low temperature range (400–500 ^{0}C), at which the calcined kaolin is comparatively reactive, hence generating a smaller amount of soluble silica; medium range (600–800 ^{0}C), at which the microspheres of kaolin have higher pore volume and a higher surface area in comparison to the later and the former; the high temperature range (800–900 ^{0}C) at which a stable reduction of active Al_2O_3 occurred and beyond 950 ^{0}C the decomposition of metakoalinite occurred. A mixture of SiO_2/Al_2O_3 having molar ratio is (Si/Al - 5) typically yield hydroxysodalite (SOD) and some other low Si/Al LTA zeolites, whereas (Si/Al -5) normally yields ZSM-11 and zeolite beta (BEA). But zeolites can be synthesized from (Si/Al > 10) having a diversity of pore sizes ranging from 0.4 to 0.8 nm. For maximum types of zeolites, NaOH of 3 M concentration is the supreme appropriate. The best temperature of crystallization for the crystalline species synthesis should be around 90^0 C and 200^0 C, but the time of crystallization should not beyond 120 h because it will form hydroxysodalite with a molar ratio of Si/Al - 5, which should perfectly yield

greater siliceous zeolite (ZSM or BEA.). Hence the zeolite synthesis at appropriate conditions can open many routes to several types of great applications if proper studies should do on it [2].

O. B. Kotova et al. studied that the fly ash (combustion of coal) produces heat and energy, is an industrialized waste, and creates a severe environmental hazard. So, to decrease the environmental load and expand the economic profits of energy production, the industry and science emphasis on the renovation of combustion of coal derivatives into new useful materials. Through the hydrothermal treatment, numerous zeolites types were produced from the fly ash. The final item for consumption was powder: mixture of zeolite and unreacted remainder in numerous ratios produced 70–80% by weight of preliminary fly ash. The experimental settings (temperature, alkali concentration and reaction time) and their quantities in the reaction products have an important impact on the zeolites types. The sequences of experiments produced the estimated crystallization pitch of zeolites and also other phases [42].

P.r Mishra et al. studied that the improvement of modular PEC solar cells for the production of hydrogen was aimed. Photo electrodes as nanostructured TiO_2 film over the Ti-metal base are manufactured by method of alkoxide sol–gel by consuming Ti $[OCH (CH_3)_2]_4$ as a precursor trailed by deposition via spin on technique for the fabrication of cell. Microstructure of the deposited film and crystalline phase have inspected through TEM and XRD. The photoelectrochemical reaction of the separate film electrodes having different areas and corresponding arrangement of two and four electrodes have noted and were compared by using 1.0 M NaOH as an electrolyte and conservative three electrode conformation. The efficiencies of photo conversion have recorded and equated for both of the conformations. The hydrogen production rates have been recorded by determining gas volume evolved over the cathode. The finest area of the photoelectrode for the design of modular PEC solar cell relates to ∼0.40 cm^2 in the present-day study [43].

Xiaoxin Zouc and Yu Zhang*ab studied that the future economy of hydrogen is a suggested system of transporting and storing energy by consuming hydrogen. During the cycle of hydrogen energy, there are three key routes: splitting of water into oxygen and

hydrogen by consuming renewable energy, collecting renewable energy (e.g., wind and solar), and recirculating working energy by the reaction of O_2 with H_2 as shown in the above Fig. The developments on the electrocatalysts which evolves hydrogen for effective water splitting (i.e., process II) was highlighted. Water splitting for maintainable production of hydrogen can find extensive range of marketable uses with both environmental and economic benefits.

On one side, the electrochemical water splitting efficiency was not only determined by the electrocatalyst oxygen evolution and hydrogen evolution reaction (HER) themselves but also their compatibility. On the other side, the photocatalytic or photoelectrochemical water splitting efficiency was also intensely affected by an appropriate combination of semiconductor materials and HER electrocatalysts. So, HER electrocatalyst is essential to be in a real electrochemical, or PEC water splitting system [44].

Yichuan Ling et al. studied that the nanocorals and Sn-doped hematite nanowires were synthesized on the FTO substrate via hydrothermal treatment and sintering at high temperature in air. These Sn-doped hematite nanostructures as compared to undoped hematite nanostructures, displayed incredible photocurrent densities in the result of enhanced structural morphology and carrier density because of Sn-doping. By adjusting Sn dopant level at low temperatures of sintering and pairing them with effective oxygen evolving catalysts make additional enhancement of photoelectrochemical presentations of these hematite nanostructures.

Additionally, studies of ultrafast laser spectroscopy showed that an important hole-electron recombination in few picoseconds caused by a high density band gap levels because of internal or surface defects. There is a longer-lived component, smaller amplitude which is liable for photocurrent that is observed in photoelectrochemical studies.

Surface morphology and Sn doping have an unimportant effect on prompt time dynamics of charge carriers that is photoexcited but have an important impact on the results of photoelectrochemical which shows that their effects are mainly important on lengthier time scale. In order to attain the lifetime of lengthier charge carrier that is photoexcited,

more research efforts should be done to increase the intrinsic electronic structure of hematite nanomaterials [45].

MATERIALS AND METHODS

3.1 Materials

The chemicals used in the synthesis of Ni-Pd decorated Sodium aluminosilicate are as follows:

Aluminum isopropoxide (AIP, 95% Daejung korea), tetraethyl orthosilicate (TEOS, 98.5% Daejung korea), tetrapropylammonium hydroxide (TPAOH, 1.0 M in H_2O Macklin), sodium hydroxide (NaOH, sigma aldrich), nickel nitrate hexahydrate $(Ni(NO_3)_2.6H_2O, 96\%)$, palladium nitrate $(Pd(NO_3)_2, 40\%$ Pd Merck Germany), deionized water, methanol (≥99.8% sigma Aldrich). All chemicals were used as received.
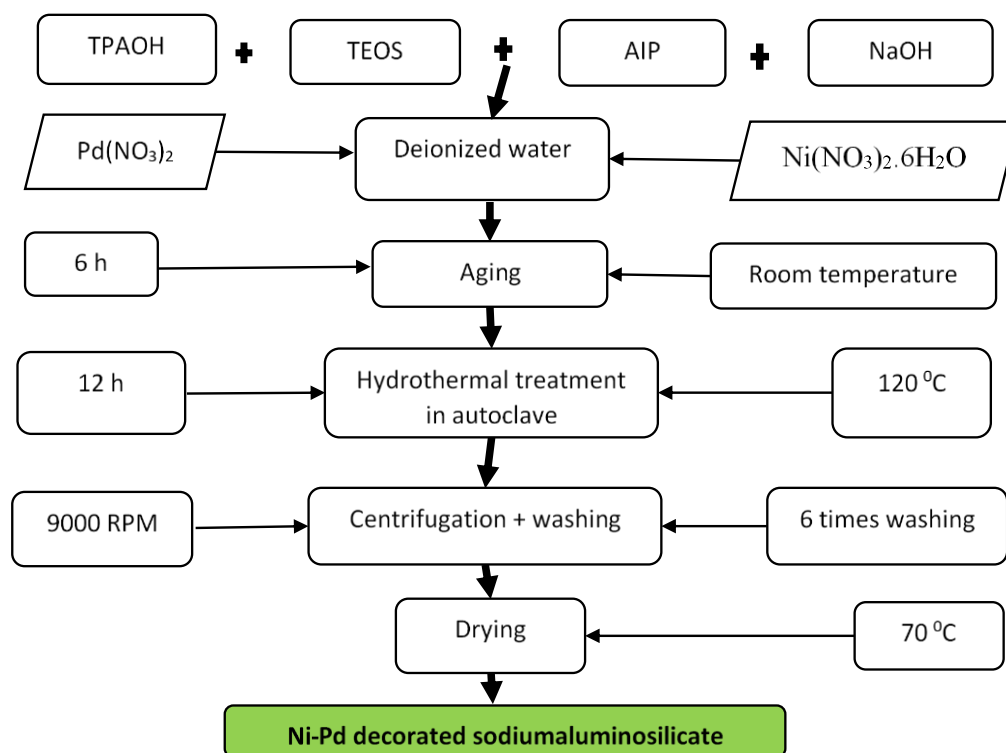
3.2 Synthesis

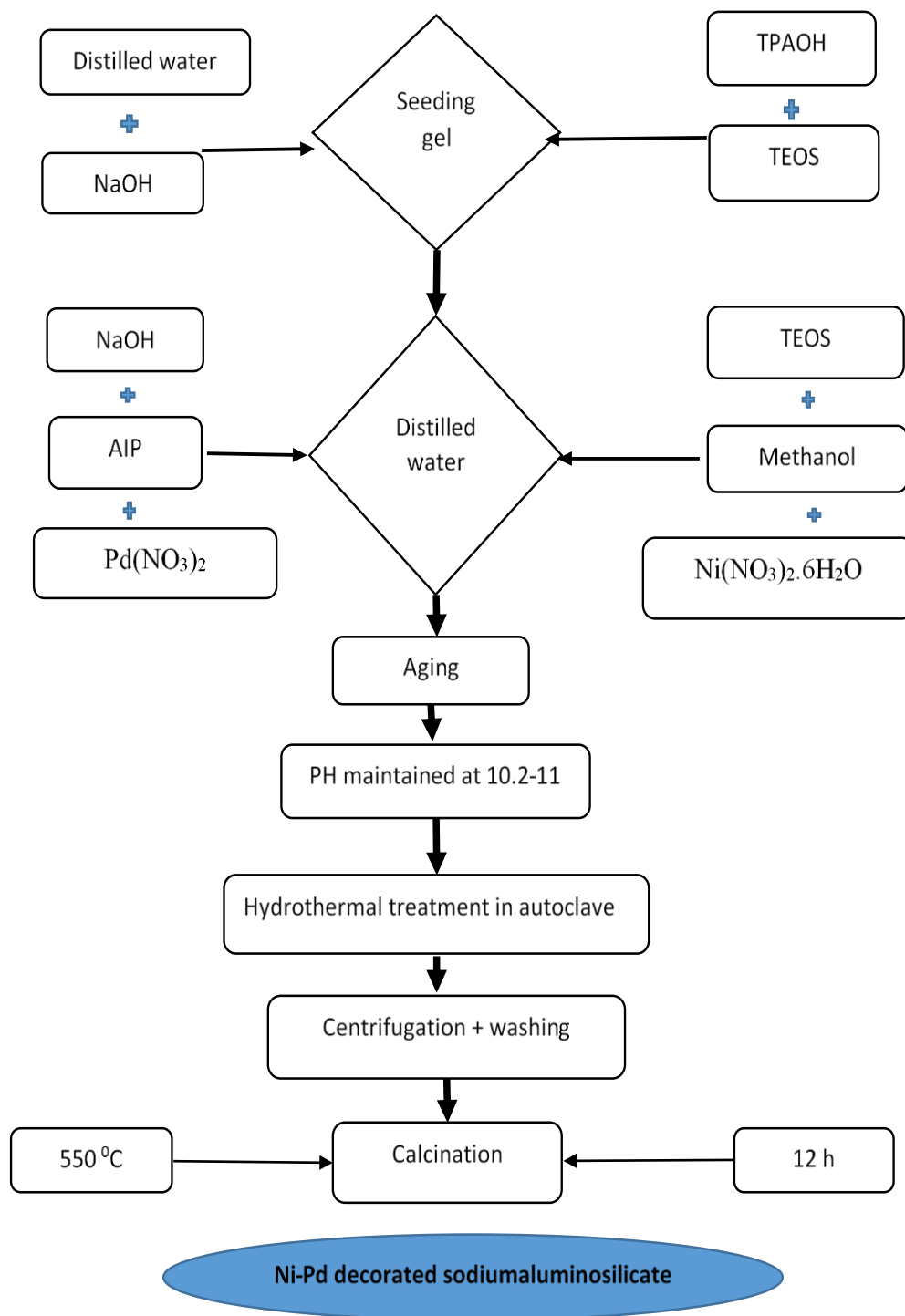**Figure 11: Flow chart of successful synthesis of Ni-Pd decorated sodiumaluminosilicate**

Figure 12: flow chart of unsuccessful synthesis of Ni-Pd decorated sodiumaluminosilicate

3.2.1 Synthesis of sodiumaluminosilicate decorated with Ni-Pd

37.5mL deionized water was taken in a 500mL beaker. 1mL tetrapropylammonium hydroxide and 13.96 ml tetraethyl orthosilicate were added dropwise to the beaker. 0.29 g of sodium hydroxide and 0.175 g of aluminum isopropoxide were added to the deionized water. 0.112g/mL of palladium nitrate and 0.12 g/10 mL of nickel nitrate were added to the mixture. The whole mixture was agitated for 6 hours. The obtained mixture was charged into 40mL Teflon tube properly sealed for hydrothermal reaction and placed in the oven at 120^0C for 12 hours. The temperature of the oven was lowered to room temperature to obtain gelatinous material. The obtained gelatinous material was separated by centrifugation at high RPM Ca. 9000 followed by washing 6 times with deionized water and dried in an oven at 70 ^{0}C until constant weight obtained.
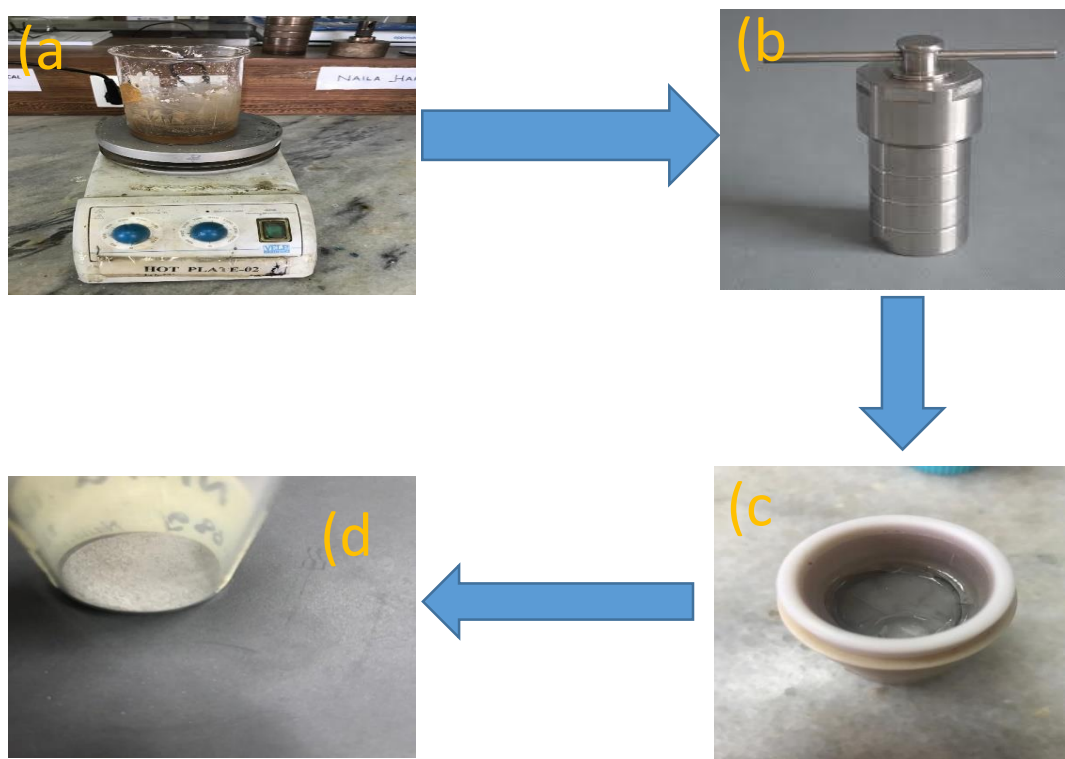

Figure 13: Schematic presentation of hydrothermal method for the synthesis of Ni-Pd decorated sodiumaluminosilicate (a) in-situ mixture of all chemical including metals (b) mixture in autoclave kept in oven (c) gelatinous material (d) prepared sample after washing

This synthesis method comprised preparation of seeding gel and In-situ encapsulation of metals are as follows:

The synthesis of seeding gel was as follows:

71.028mL (3.946 mole) of distilled water was taken in a beaker and 0.6 g (0.01725 mole) of sodium hydroxide was added in distilled water and dissolved it. 27.7mL (0.02875 mole) of tetra propylammonium hydroxide was added dropwise into the mixture with continuous stirring for at least 30 min followed by dropwise addition of 27.5mL (0.1322 mole) of tetraethyl orthosilicate to the mixture. The entire mixture was stirred at 100 ^{0}C for approximately 16 h and then this mixture was utilized as seeding gel.

The synthesis of Ni-Pd decorated sodiumaluminosilicate was as follows:

0.29 g of sodium hydroxide was dissolved in a given 20mL distilled water. 0.35g of aluminum isopropoxide and 65.3mL of methanol as a solvent were added into the mixture and stirred for approximately 30 min followed by the dropwise addition of 13.96mL of Tetraethyl orthosilicate and was stirred for an hour. 0.24g/10 mL of nickel nitrate and 0.22g/10 mL of Palladium nitrate were added into the mixture. Lastly, 5 g of seeding gel was used in the mixture followed by stirring for 1 h. The mixture pH was maintained between 10.2–11.0. The total mixture was transferred to 40mL Parr autoclave and stirring was done at different temperatures such as 250 ^{0}C, 180 ^{0}C, 140 ^{0}C, and 120 ^{0}C for 10h, 24h and 5 days, 6 days, 7 days and 12h respectively. The obtained solid product was followed by filtration, washing with distilled water and dried at 100-110 ^{0}C for 6 h. The calcination was done at 550 ^{0}C for 12 h in chamber furnace for removing the organic templates.

3.2.2 Synthesis of thin film

Fluorine doped Tin Oxide (FTO 2×1 cm) glass was washed with double distilled water, then with acetone, propanol and ethanol and dried. 0.3 milligrams of sample dissolved in 3 mL methanol. Then the mixture was sonicated for 30 mins. The multimeter was used to check the conductive side of the FTO. The thin film was deposited by drop casting

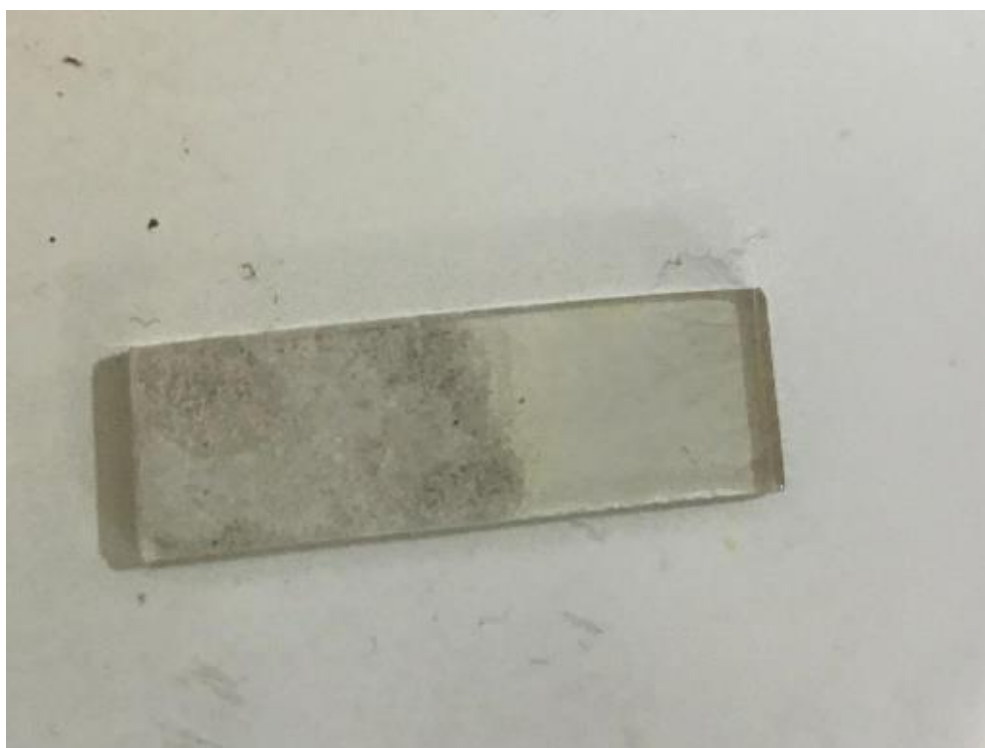method on the conducting side of FTO and then few drops of Nafion binder were added and air dried.

Figure 14: As synthesized FTO glass

RESULTS AND DISCUSSIONS

4.1   Diffuse Reflectance Spectroscopy (DRS) and Tauc plot

The diffused reflectance spectrum (DRUV-Vis) of Ni-Pd decorated Sodiumaluminosilicate is shown in figure 13. The spectrum indicates absorbance edge at 260 nm. The energy associates with this absorption edge yield band gap energy value of 4.5 eV calculated from tauc plot showing potential of the material as photo catalyst. Tauc plot was plotted between $(\alpha h\nu)^2$ and photon energy for the calculation of band gaps of the prepared sample of Ni-Pd decorated Sodium aluminosilicate. The spectrum shows the least absorbance edge as it has the higher band gap so as a result, it can capture photons in ultraviolet and visible region to generate electrons and holes efficiently. It can be useful for photoelectrochemical applications.
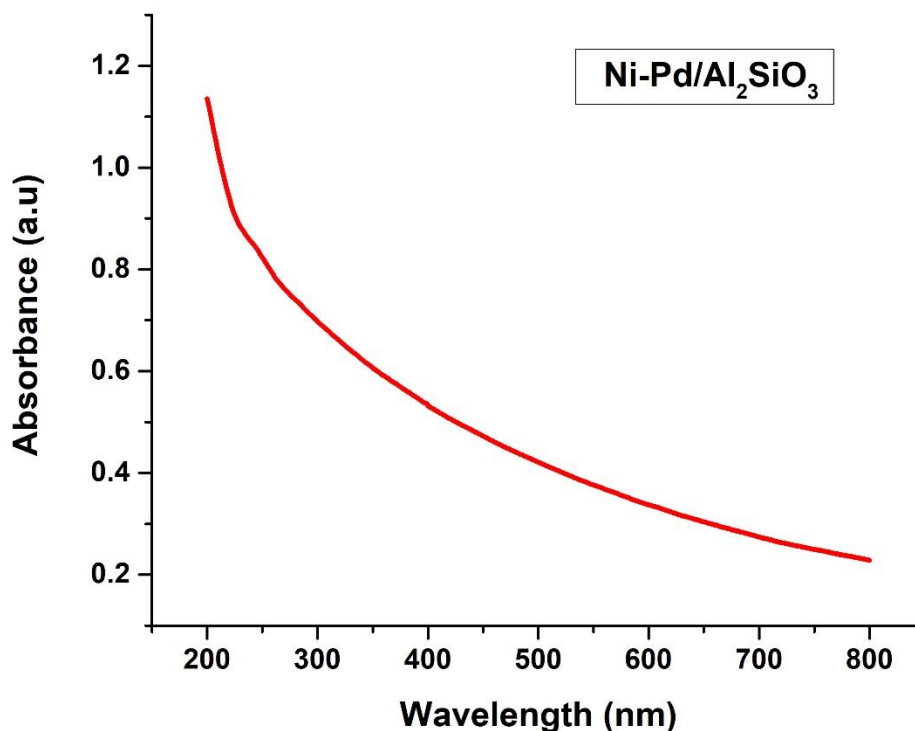

Figure 15: DRUV−visible spectra of Ni-Pd decorated Sodium aluminosilicate
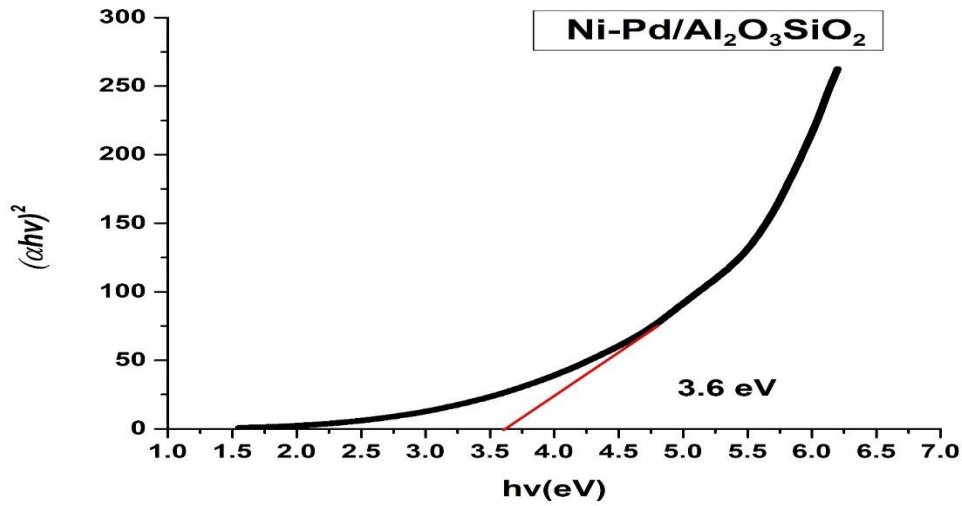
Figure 16: Estimated band gap energy of Ni-Pd decorated Sodiumaluminosilicate

4.2 Fourier Transform Infrared Spectroscopy (FTIR) results

The IR spectrum of Ni-Pd decorated sodiumaluminosilicate is shown in figure 14.
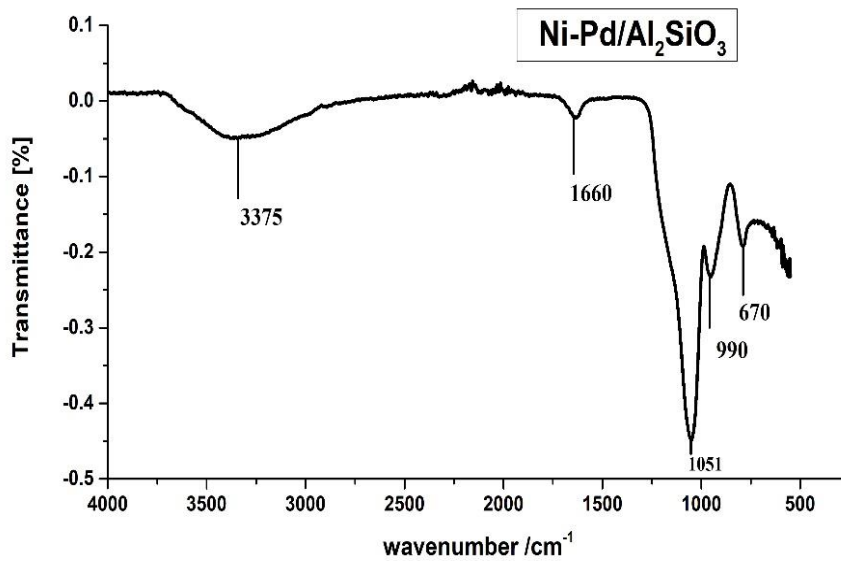

Figure 17: FTIR spectrum of Ni-Pd decorated sodiumaluminosilicate showing presence of vibrational frequency of Al-O-Si, Si-O-Si, Si-OH, H2O and SiOH bonds

The assignments of the observed vibrational frequencies are tabulated in table 2.

Table 1: IR bands of Ni-Pd decorated sodiumaluminosilicate with their possible assignments

S. No	Vibrational frequency (cm^{-1})	Assignment
1	3375	OH groups of Si-OH and adsorbed water molecules on the surface Ni-Pd decorated sodiumaluminosilicate
2	1660	Stretching of H-O-H
3	1051	Al-O-Si asymmetric streching
4	990	Si-O-Si asymmetric streching
5	670	Al-O bending vibration

4.3 X- ray diffraction (XRD) results

The plain materials of sodiumaluminosilicate have an amorphous appeal. The X- ray diffraction (XRD) pattern of synthesized sodiumaluminosilicate is shown in Figure 18, which demonstrates the presence of crystalline phases in the sample. The XRD shows presence of crystalline quartz, alumina and aluminosilicate. The quartz exhibits 2θ values as broad peaks at 22.43°, 40.66°, 49.96° of 2θ values and d spacing of 4.28, 3.36, 3.34, 2.21, 1,82 Å. The 2θ values in the region between 14^0 and 30^0 shows presence of amorphous phases of silica and alumina present in the bulk material. The presence of Nickel and Palladium in the sodiumaluminosilicate is indicated by the 2θ values at 37.2^0, 43.2^0, 62.8^0 and 42.3^0 respectively. The small diffraction peaks that appear in the diffractogram are due to presence of small amount of Ni and Pd distributed uniformly all over the structure. All the assignments agree with the literature value [46].
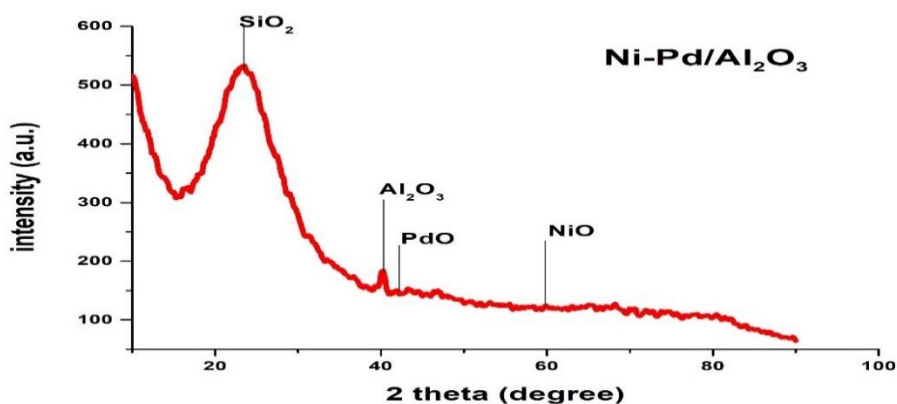
Figure 18: XRD pattern depicting major contents of silicate structure in sodiumaluminosilicate

4.4 Thermogravimetric analysis(TGA) results

To check the volatile matter presence in Ni-Pd decorated sodiumaluminosilicate, TGA was performed. The measurements were done at the heating rate of 10 C/min, hold temp and time were 600 ^{0}C for 2 min under the inert atmosphere of flowing dinitrogen gas at the rate of 50 mL/min. The thermogram indicates that there is no loss of water and the product is stable up to 600 ^{0}C.
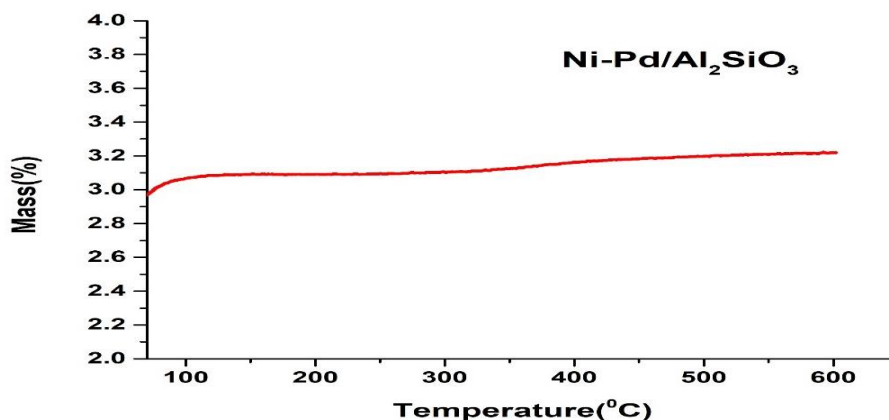

Figure 19: TGA graph at the rate 10 C/min to 600 ^{0}C

4.5 Scanning Electron Microscope (SEM) results

Surface/crystal morphology/texture features were studied by scanning electron microscope. The SEM images of the sample (Sodiumaluminosilicate) decorated with Ni.

.and Pd particles are shown in the figure. Particle sizes of the sample were calculated by SEM and was found to be 193 nm to 48.01 nm. Further the SEM images show layered structure having canals, pores and voids in between the layers with homogeneously distributed Nickel and Palladium particles .
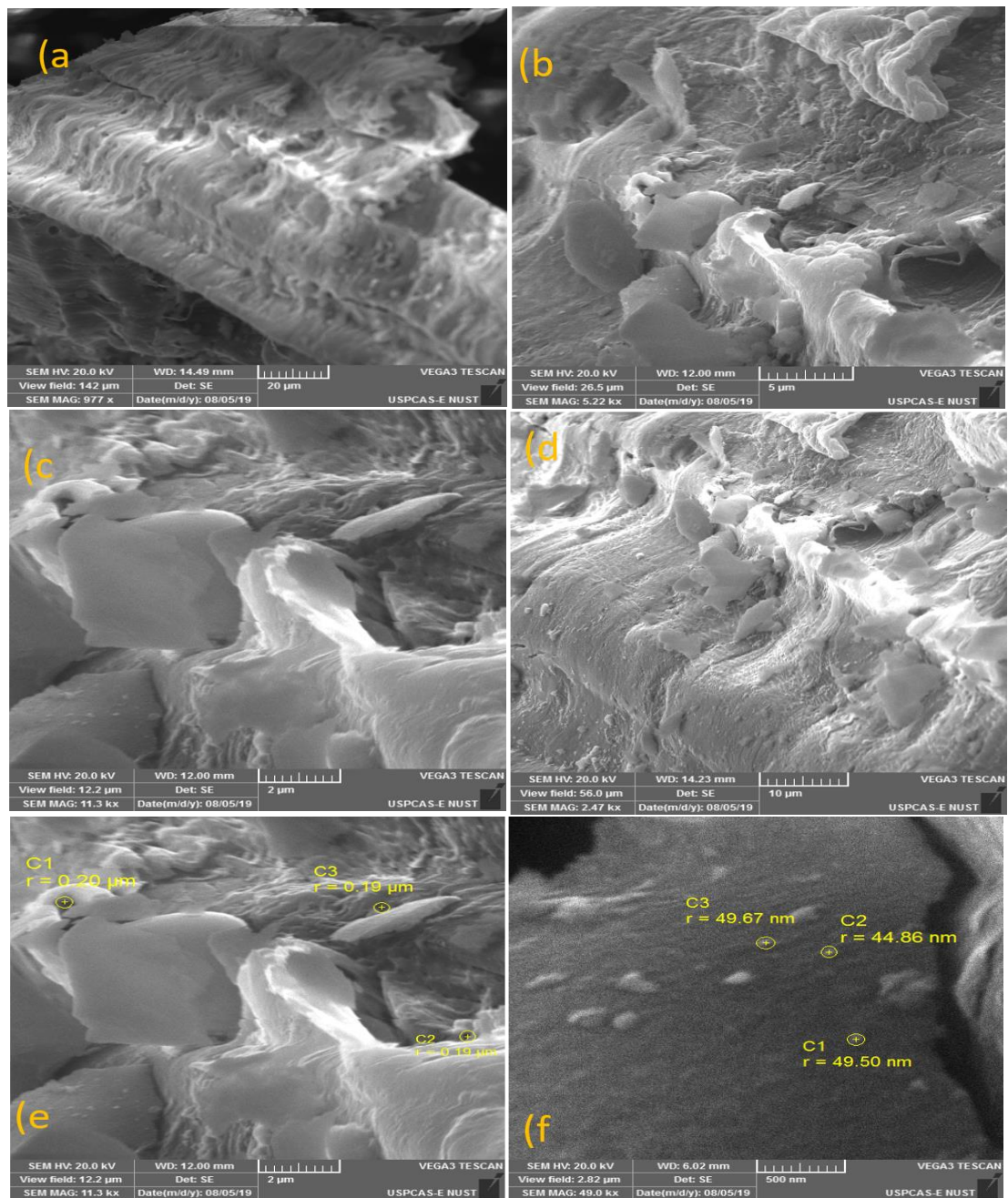

Figure 20: SEM images of Ni and Pd nanoparticles decorated sodiumaluminosilicate showing layered structures having channels and pores in between the layers

4.6 Energy dispersive x-ray (EDS) analysis

The elemental composition of the sample was studied by energy dispersive X-rays analysis. The elements Na, Al, Si, O, Ni, Pd are present in weight % and atomic% in the given below table. There seems to be presence of carbonaceous impurity from the starting materials. Only catalytic amount of 1% of Ni and Pd used to decorate the sodiumaluminosilicate, therefore both of these metals are not detectable in EDS analysis. The remaining all the elements that constitute bulk material have been found to be present.

Table 2a: Elemental composition of Ni-Pd decorated Sodiumaluminosilicate

Element	Weight %	Atomic %
C	10.97	15.85
O	62.32	67.64
Na	0.01	0.01
Al	0.83	0.53
Si	25.80	15.95
Ni	0.05	0.02
Pd	0.03	0.00
Total	100.00	

Table 2b: Elemental Composition of Ni-Pd decorated Sodiumaluminosilicate

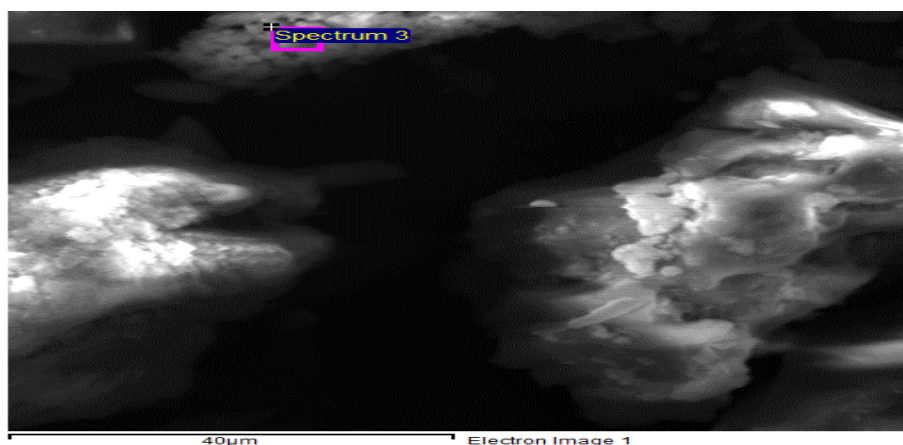| Elements	Weight %	Atomic %
C	16.49	23.27
O	57.73	61.17
Na	0.08	0.06
Al	0.50	0.31
Si	25.09	15.15
Ni	0.11	0.03
Total	100.00	

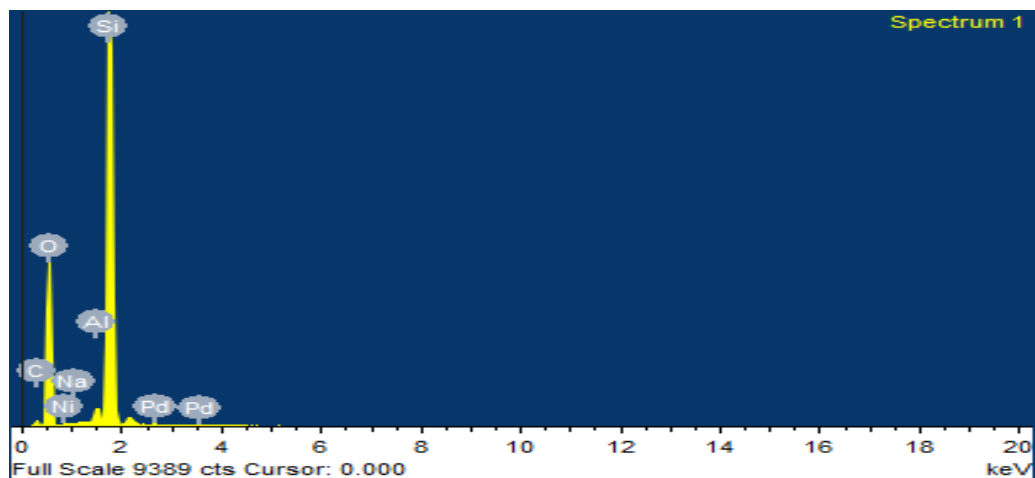**Figure 21a: SEM picture shows the location of probe**

Figure 21b: EDS spectrum of aluminosilicate decorated with Ni-P
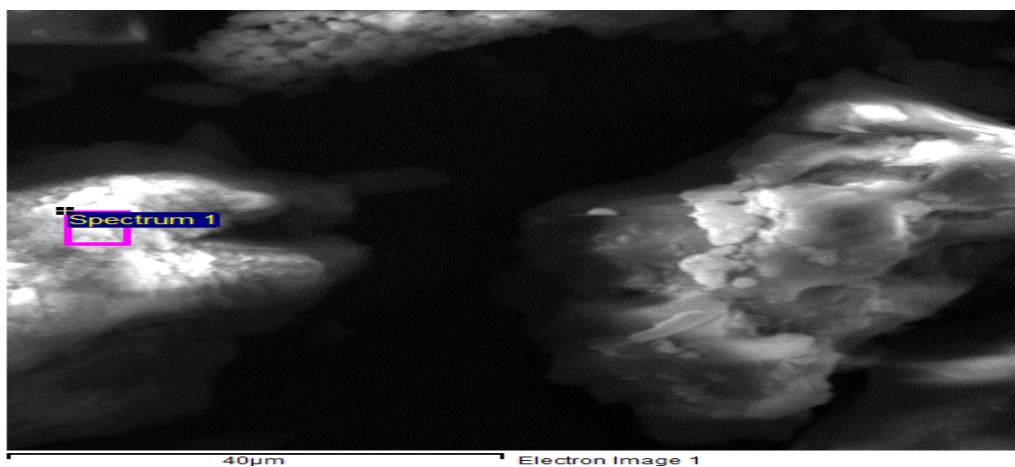

Figure 22a: SEM picture shows the location of probe
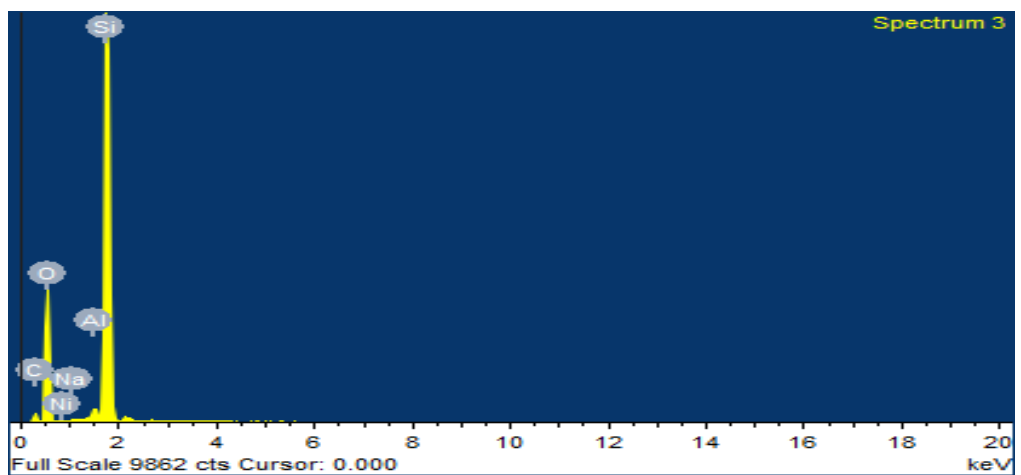

Figure 22b: EDS spectrum of aluminosilicate decorated with Ni-P

4.7 Transmission electron microscopy(TEM) results

TEM images of Ni-Pd decorated Sodium aluminosilicate showing presence of channels, pores and voids at various resolutions**.** The prepared sample seems to have tubular structure that is an intermediate step which transformed from a solid state phase to a layered mesoporous structure of sodiumaluminosilicate. The ordered porous structure of aluminosilicate is clearly visible in the fig (a) at 50 nm resolution.
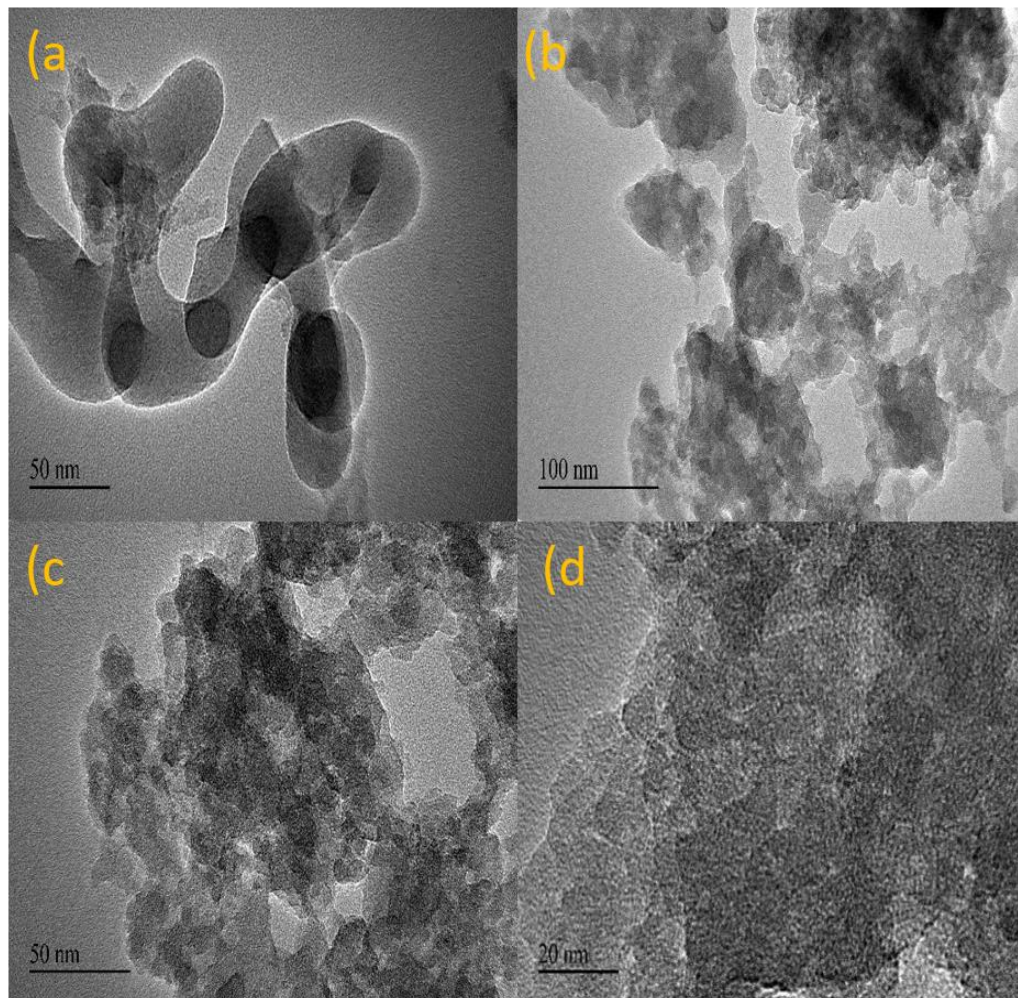

Figure 23: TEM images of Ni-Pd decorated sodiumaluminosilicate at various resolutions (a) 50 nm (b) 100 nm (c) 50 nm (d) 20 nm showing presence of channels, pores and voids

4.8 X-ray photo electron spectroscopy (XPS) Results

The elemental components and their oxidation states of Ni-Pd decorated sodiumaluminosilicate were examined by X-ray photo electron spectroscopy (XPS). The apparent survey of Ni-Pd decorated sodiumaluminosilicate confirms the presence of Al, Si, Ni, Pd, O, and C. The separate high-resolutions XPS spectrum of Al2p, Si2p, Ni2p, Pd3d, O1s, and C1s are also shown. The XPS spectrum of Al2p shows two overlap peaks at binding energies of 71.88 eV and 73.08 eV credited to Al metal and silicate respectively, Si2p shows two peaks at binding energies of 101.98 and 102.98 eV attributed to SiO_2 and aluminosilicate respectively, Pd3d shows two peaks at binding energies of 334.18 and 339.58 eV which shows the presence of $Pd3d_{3/2}$ and $Pd3d_{5/2}$, Ni2p shows an undistinguishable peak at binding energy of 854.38 eV which can be either Ni metal or Ni oxide, C1s shows two overlap peaks at binding energies of 283.88 and 289.08 eV attributed to C-C and O-C=O and O1s shows two peaks at binding energies of 532.88 and 531.88 eV (531.18 Al_2O_3 and 532.88 SiO_2) in Ni-Pd decorated Sodium aluminosilicate. The binding energies took from XPS confirms the synthesis of Ni-Pd decorated Sodium aluminosilicate [47].
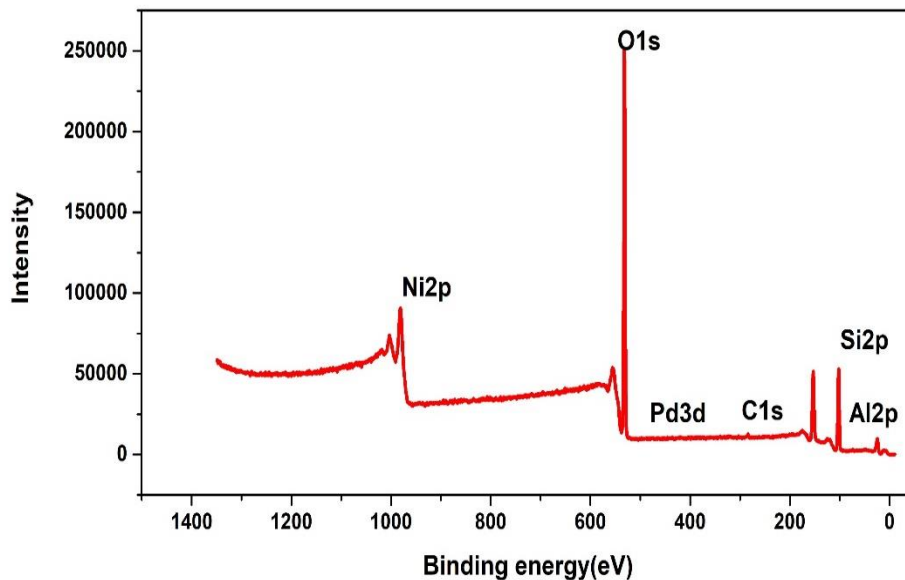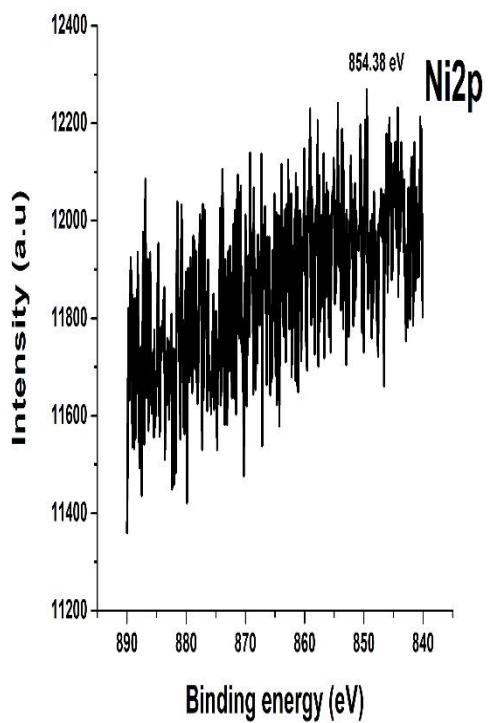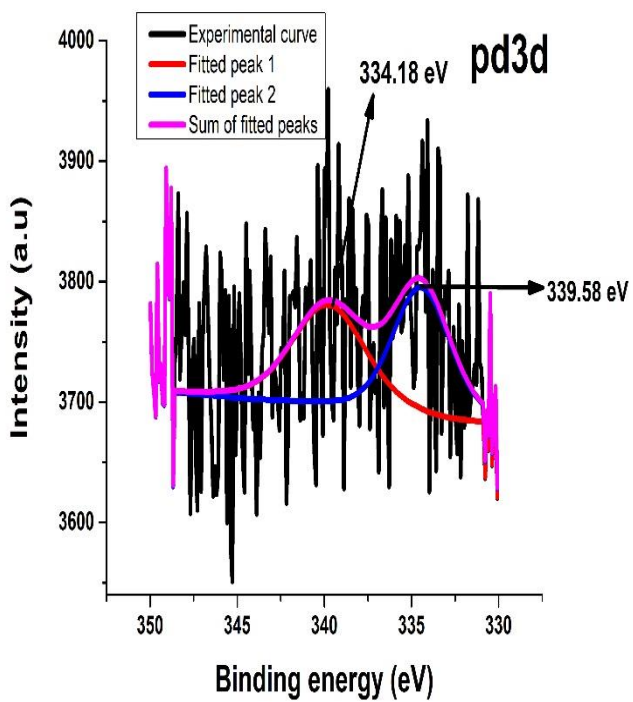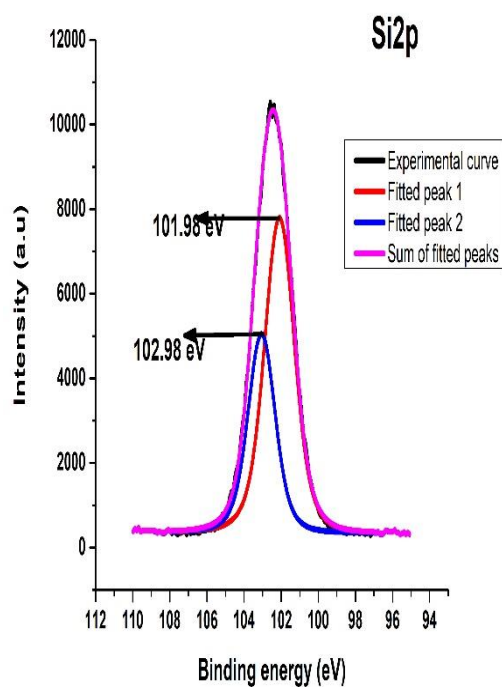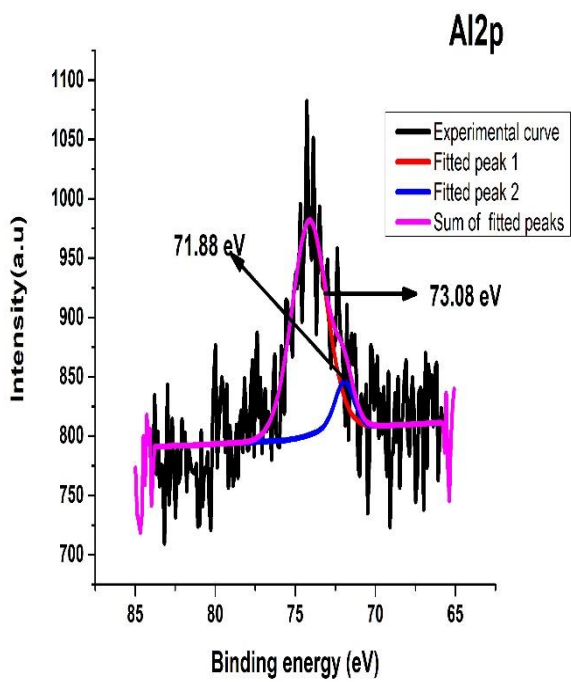

Figure 24a: Surface survey XPS image of Ni-Pd decorated sodiumaluminosilicate
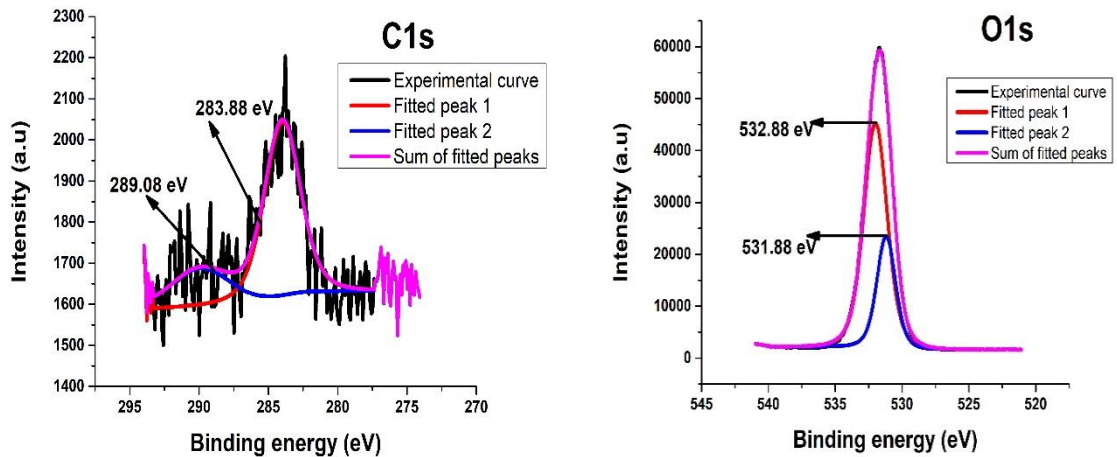
Figure 24b: High resolution spectra of Al2p, Si2p, pd3d, Ni2p, C1s and O1s

4.9 Brunauer Emmet Teller (BET) results

The external surface area of Ni-Pd decorated sodiumaluminosilicate was studied by N_2 adsorption isotherm by using the Brunauer Emmet Teller theory (BET). The sample was degassed at 120^0C in vaccum for 8 hrs in the p/p^0 range from 0.05-0.3. The surface areas of samples were calculated by the Brunauer−Emmett−Teller (BET) method. The specific micropore surface areas and pore volumes were calculated by t-plot method. The Langmuir isotherm surface area was 1230.638 m²/g. The overall BET surface area was 875.178 m²/g. The single point surface area was 862.6669 m²/g. The multi-point surface area was 875.178 m²/g. The total pore volume was 7.083e-01 cc/g for pores smaller than 2302.7 ^0A (RADIUS) at P/Po = 0.99583. The BJH desorption summary Surface Area was 285.073 m²/g, Pore Volume was 0.341 cc/g and Pore Radius Dv(r) was 19.082 Å. BJH adsorption summary Surface Area was 218.730 m²/g, Pore Volume was 0.331 c/g, and Pore Radius Dv(r) was 19.037 Å.

The increase in surface area of the samples depends on synthetic condition e.g. agitation time, temperature, reaction time etc. Metal salts were also used in very less quantity which is also one of the reason of the surface area increasing.

Table 3: Summary of all BET surface areas of Ni-Pd decorated sodiumaluminosilicate samples prepared under varying conditions of heating temperature and time.

Sample	Temperature (^{0}C)	Time	BET surface area (m^2/g)	Langmuir surface area (m^2/g)
Ni-Eu decorated sodiumaluminosilicate	250	12 h	1.7	3.420
Ni-Eu decorated sodiumaluminosilicate	180	5 days	31	33
Ni-Eu decorated sodiumaluminosilicate	180	12 h	13	15
Ni-Eu decorated sodiumaluminosilicate	140	6 days	37	39
Ni-Pd decorated sodiumaluminosilicate in inert atmosphere	120	7 days	2.7	4.280
Ni-Pd decorated sodiumaluminosilicate	120	12 h	875.18	1230.638

4.10 APPLICATIONS

4.10.1 PEC Water splitting

4.10.1.1 Chronoamperometry (CA) results

The chronoamperogram, shows good photo response of Ni-Pd decorated sodiumaluminosilicate. The current seems to be stable under light ON/OFF conditions using 0.1 KCl as an electrolyte which shows that the material is photo stable up to 600 seconds.

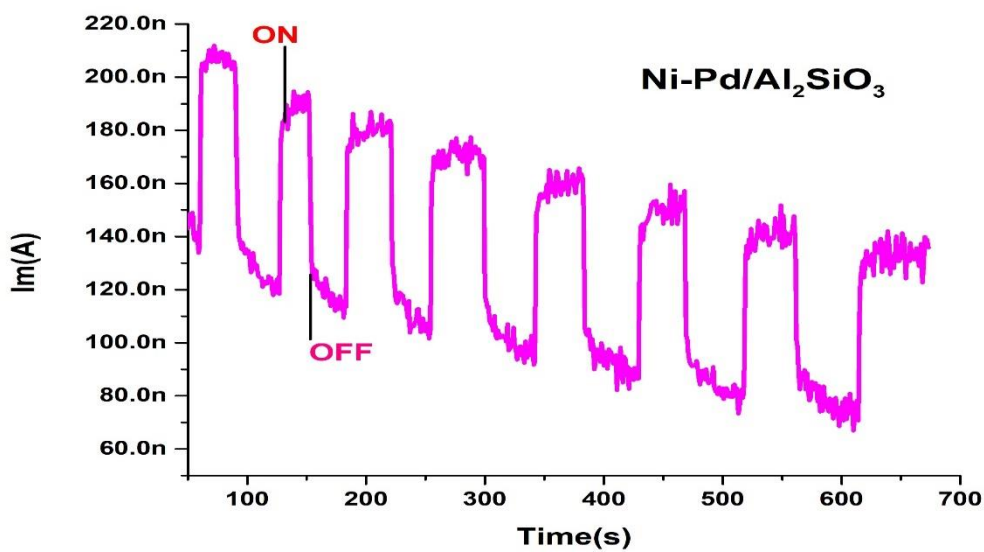**Figure 25: Chronoamperogram of Ni-Pd decorated sodiumaluminosilicate indicating stability of the material up to 600 seconds**

4.10.1.2 *Water stability results*

A plot of time vs current for sodiumaluminosilicate decorated with Ni-Pd particles show stability of photo catalyst under light ON/OFF condition using 0.1M KCl as an electrolyte.
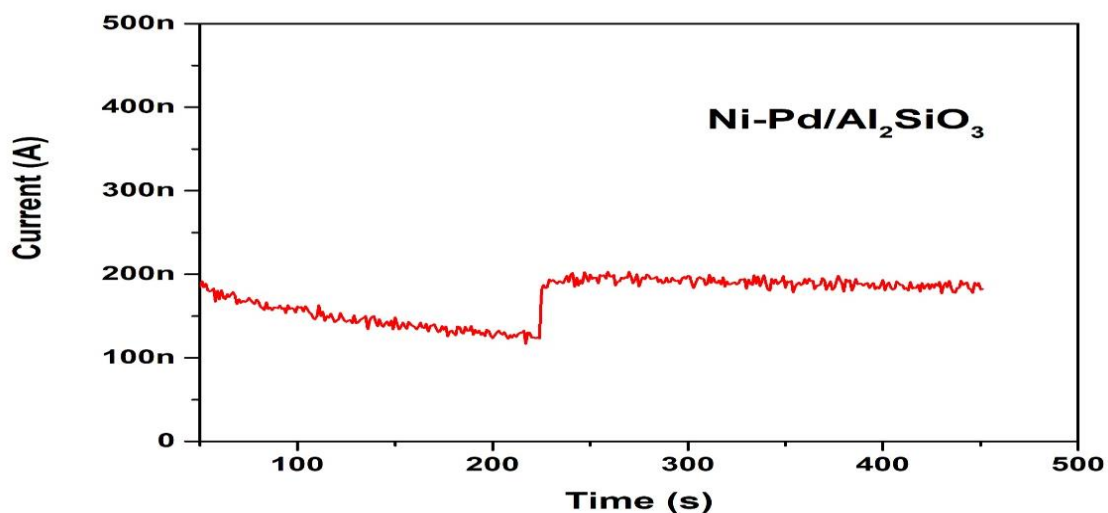

Figure 26: Water stability of the catalyst

CONCLUSION

Nickel and Palladium decorated sodiumaluminosilicate structures have been prepared by hydrothermal process at 120 ^{0}C for 12 hours. The as prepared material has been characterized by various analytical techniques such as Diffused reflectance spectroscopy (DRS), Fourier transform infrared spectroscopy (FTIR), X-ray diffraction (XRD), Thermogravimetric analysis (TG), Scanning electron microscopy (SEM), Energy dispersive spectroscopy (EDS), Transmission electron microscopy (TEM), X-ray photoelectron spectroscopy (XPS) and Brunauer-Emmett-Teller (BET). The analysis indicates presence of all the necessary ingredients in the synthesized material. The stability test carried out by TGA showed no loss in weight up to 600 ^{0}C. The SEM and TEM shows layered structure having canals, pores and voids in between the layers with homogenously distribution of nickel and palladium in the bulk material. The BET and Langmuir surface areas were found to be 875.178 and 1230.638 m^2/g respectively indicating possible use of the material as photo catalyst, hydrogen storage material and hydrocarbon modification. The material has been found to be stable under all operational conditions, non-degradable and cost effective.

REFERENCES

1. Umeda, T., Yamada, H., Ohara, K., Yoshida, K., Sasaki, Y., Takano, M., ... & Wakihara, T. (2017). Comparative study on the different interaction pathways between amorphous aluminosilicate species and organic structure-directing agents yielding different zeolite Phases. *The Journal of Physical Chemistry C*, *121*(43), 24324-24334.

2. Abdullahi, T., Harun, Z., & Othman, M. H. D. (2017). A review on sustainable synthesis of zeolite from kaolinite resources via hydrothermal process. *Advanced Powder Technology*, *28*(8), 1827-1840.

3. Li, Y., & Yu, J. (2014). New stories of zeolite structures: their descriptions, determinations, predictions, and evaluations. *Chemical reviews*, *114*(14), 7268-7316.

4. Marcos-Hernández, M., & Villagrán, D. (2019). Mesoporous Composite Nanomaterials for Dye Removal and Other Applications. In *Composite Nanoadsorbents* (pp. 265-293). Elsevier.

5. Marcos-Hernández, M., & Villagrán, D. (2019). Mesoporous composite nanomaterials for dye removal and other applications. In *Composite Nanoadsorbents* (pp. 265-293). Elsevier.

6. Moeller. T (1952). Inorganic chemistry. An advanced textbook: (PP. 721-729) John Wiley and Sons, Inc., New York.

7. Dusselier, M., & Davis, M. E. (2018). Small-pore zeolites: synthesis and catalysis. *Chemical reviews*, *118*(11), 5265-5329.

8. Yue, Y., Gu, L., Zhou, Y., Liu, H., Yuan, P., Zhu, H., ... & Bao, X. (2017). Template-free synthesis and catalytic applications of microporous and hierarchical ZSM-5 zeolites from natural aluminosilicate minerals. *Industrial & Engineering Chemistry Research*, *56*(36), 10069-10077.

9. Ikuno, T., Chaikittisilp, W., Liu, Z., Iida, T., Yanaba, Y., Yoshikawa, T., ... & Okubo, T. (2015). Structure-directing behaviors of tetraethylammonium cations toward zeolite beta revealed by the evolution of aluminosilicate species formed

during the crystallization process. *Journal of the American Chemical Society*, *137*(45), 14533-14544.

10. Otto, T., Zones, S. I., & Iglesia, E. (2018). Synthetic strategies for the encapsulation of nanoparticles of Ni, Co, and Fe oxides within crystalline microporous aluminosilicates. *Microporous and Mesoporous Materials*, *270*, 10-23.

11. Broom, D. P., Webb, C. J., Fanourgakis, G. S., Froudakis, G. E., Trikalitis, P. N., & Hirscher, M. (2019). Concepts for improving hydrogen storage in nanoporous materials. *International Journal of Hydrogen Energy*, *44*(15), 7768-7779.

12. Li, Z., Luo, W., Zhang, M., Feng, J., & Zou, Z. (2013). Photoelectrochemical cells for solar hydrogen production: current state of promising photoelectrodes, methods to improve their properties, and outlook. *Energy & Environmental Science*, *6*(2), 347-370.

13. Bak, T., Nowotny, J., Rekas, M., & Sorrell, C. C. (2002). Photo-electrochemical hydrogen generation from water using solar energy. Materials-related aspects. *International journal of hydrogen energy*, *27*(10), 991-1022.

14. Walter, M. G., Warren, E. L., McKone, J. R., Boettcher, S. W., Mi, Q., Santori, E. A., & Lewis, N. S. (2010). Solar water splitting cells. *Chemical reviews*, *110*(11), 6446-6473.

15. Rai, S., Ikram, A., Sahai, S., Dass, S., Shrivastav, R., & Satsangi, V. R. (2017). CNT based photoelectrodes for PEC generation of hydrogen: a review. *International Journal of Hydrogen Energy*, *42*(7), 3994-4006.

16. Maeda, K., & Domen, K. (2010). Photocatalytic water splitting: recent progress and future challenges. *The Journal of Physical Chemistry Letters*, *1*(18), 2655-2661.

17. Walter, M. G., Warren, E. L., McKone, J. R., Boettcher, S. W., Mi, Q., Santori, E. A., & Lewis, N. S. (2010). Solar water splitting cells. *Chemical reviews*, *110*(11), 6446-6473.

18. Kudo, A., & Miseki, Y. (2009). Heterogeneous photocatalyst materials for water splitting. *Chemical Society Reviews*, *38*(1), 253-278.

19. Hisatomi, T., Kubota, J., & Domen, K. (2014). Recent advances in semiconductors for photocatalytic and photoelectrochemical water splitting. *Chemical Society Reviews*, *43*(22), 7520-7535.

20. Chen, Z., Jaramillo, T. F., Deutsch, T. G., Kleiman-Shwarsctein, A., Forman, A. J., Gaillard, N., ... & McFarland, E. W. (2010). Accelerating materials development for photoelectrochemical hydrogen production: Standards for methods, definitions, and reporting protocols. *Journal of Materials Research*, *25*(1), 3-16.

21. Maeda, K. (2013). Z-scheme water splitting using two different semiconductor photocatalysts. *Acs Catalysis*, *3*(7), 1486-1503.

22. Sivula, K., Le Formal, F., & Grätzel, M. (2011). Solar water splitting: progress using hematite (α-Fe2O3) photoelectrodes. *ChemSusChem*, *4*(4), 432-449.

23. Maeda, K., & Domen, K. (2007). New non-oxide photocatalysts designed for overall water splitting under visible light. *The Journal of Physical Chemistry C*, *111*(22), 7851-7861.

24. Moriya, Y., Takata, T., & Domen, K. (2013). Recent progress in the development of (oxy) nitride photocatalysts for water splitting under visible-light irradiation. *Coordination Chemistry Reviews*, *257*(13-14), 1957-1969.

25. Takanabe, K., & Domen, K. (2012). Preparation of inorganic photocatalytic materials for overall water splitting. *ChemCatChem*, *4*(10), 1485-1497.

26. Osterloh, F. E. (2013). Inorganic nanostructures for photoelectrochemical and photocatalytic water splitting. *Chemical Society Reviews*, *42*(6), 2294-2320.

27. Hisatomi, T., Minegishi, T., & Domen, K. (2012). Kinetic assessment and numerical modeling of photocatalytic water splitting toward efficient solar hydrogen production. *Bulletin of the Chemical Society of Japan*, *85*(6), 647-655.

28. Tachibana, Y., Vayssieres, L., & Durrant, J. R. (2012). Artificial photosynthesis for solar water-splitting. *Nature Photonics*, *6*(8), 511.

29. Kristo, M. J. (2012). Nuclear forensics. In Handbook of Radioactivity Analysis (Third Edition): (pp. 1281-1304). Lawrence Livermore National Laboratory, Livermore, CA, USA

30. González-García, P. (2018). Activated carbon from lignocellulosics precursors: A review of the synthesis methods, characterization techniques and applications. *Renewable and Sustainable Energy Reviews*, *82*, 1393-1414.

31. Stuart, B. H. (2007). *Analytical techniques in materials conservation*. John Wiley & Sons.

32. Crankovic, G. M. Volume 10: Materials Characterization (Asm Handbook) (ASM International, 1986).

33. Hayashi, J. I., Horikawa, T., Takeda, I., Muroyama, K., & Ani, F. N. (2002). Preparing activated carbon from various nutshells by chemical activation with K2CO3. *Carbon*, *40*(13), 2381-2386.

34. Lozano-Castello, D., Lillo-Rodenas, M. A., Cazorla-Amorós, D., & Linares-Solano, A. (2001). Preparation of activated carbons from Spanish anthracite: I. Activation by KOH. *Carbon*, *39*(5), 741-749.

35. Cazetta, A. L., Vargas, A. M., Nogami, E. M., Kunita, M. H., Guilherme, M. R., Martins, A. C., ... & Almeida, V. C. (2011). NaOH-activated carbon of high surface area produced from coconut shell: Kinetics and equilibrium studies from the methylene blue adsorption. *Chemical Engineering Journal*, *174*(1), 117-125.

36. Foo, K. Y., & Hameed, B. H. (2011). Preparation and characterization of activated carbon from pistachio nut shells via microwave-induced chemical activation. *Biomass and Bioenergy*, *35*(7), 3257-3261.

37. Rivera-Utrilla, J., Sánchez-Polo, M., Gómez-Serrano, V., Alvarez, P. M., Alvim-Ferraz, M. C. M., & Dias, J. M. (2011). Activated carbon modifications to enhance its water treatment applications. An overview. *Journal of hazardous materials*, *187*(1-3), 1-23.

38. Martins, M. C. L., Fonseca, C., Barbosa, M. A., & Ratner, B. D. (2003). Albumin adsorption on alkanethiols self-assembled monolayers on gold electrodes studied by chronopotentiometry. *Biomaterials*, *24*(21), 3697-3706.

39. Wang, H., Lin, H. J., Cai, W. T., Ouyang, L. Z., & Zhu, M. (2016). Tuning kinetics and thermodynamics of hydrogen storage in light metal element based systems–a review of recent progress. *Journal of Alloys and Compounds*, *658*, 280-300.

40. Barthelemy, H., Weber, M., & Barbier, F. (2017). Hydrogen storage: recent improvements and industrial perspectives. *International Journal of Hydrogen Energy*, *42*(11), 7254-7262.

41. Johnson, E. B. G., & Arshad, S. E. (2014). Hydrothermally synthesized zeolites based on kaolinite: a review. *Applied Clay Science*, *97*, 215-221.

42. Kotova, O. B., Shabalin, I. N., Shushkov, D. A., & Kocheva, L. S. (2016). Hydrothermal synthesis of zeolites from coal fly ash. *Advances in Applied Ceramics*, *115*(3), 152-157.

43. Mishra, P. R., Shukla, P. K., & Srivastava, O. N. (2007). Study of modular PEC solar cells for photoelectrochemical splitting of water employing nanostructured TiO2 photoelectrodes. *International Journal of Hydrogen Energy*, *32*(12), 1680-1685.

44. Zou, X., & Zhang, Y. (2015). Noble metal-free hydrogen evolution catalysts for water splitting. *Chemical Society Reviews*, *44*(15), 5148-5180.

45. Ling, Y., Wang, G., Wheeler, D. A., Zhang, J. Z., & Li, Y. (2011). Sn-doped hematite nanostructures for photoelectrochemical water splitting. *Nano letters*, *11*(5), 2119-2125.

46. Alehyen, S., Achouri, M. E. L., & Taibi, M. (2017). Characterization, microstructure and properties of fly ash-based geopolymer. *J. Mater. Environ. Sci*, *8*(5), 1783-1796.

47. Todea, M., Vanea, E., Bran, S., Berce, P., & Simon, S. (2013). XPS analysis of aluminosilicate microspheres bioactivity tested in vitro. *Applied Surface Science*, *270*, 777-783.